University of California
Santa Barbara

Touch Amplification for Human Computer Interaction

A thesis submitted in partial satisfaction
of the requirements for the degree

Master of Science
in
Electrical and Computer Engineering

by

Harald Schäfer

Committee in charge:

Professor Yon Visell, Chair
Professor Matthew Turk
Professor Andrew Teel

June 2017

The Thesis of Harald Schäfer is approved.

Professor Matthew Turk

Professor Andrew Teel

Professor Yon Visell, Committee Chair

May 2017

Touch Amplification for Human Computer Interaction

by

Harald Schäfer

Acknowledgements

This thesis would not have been possible without the invaluable support that I have received from friends, family and colleagues.

I would like to thank the committee members, Matthew Turk and Andrew Teel, for serving on the committee and their willingness to give advice.

Working in the Re-touch lab has been a great honor and pleasure. I am thankful for the incredible opportunity to work alongside knowledgeable people that are always eager to help and collaborate.

Most importantly, I would like to thank my advisor, Prof. Yon Visell, director and principal investigator of the Re-touch lab in University of California Santa Barbara. The continual support and advice he has provided has been essential for the completion of this thesis. His passion for research is truly inspiring. Despite busy schedules, professor Visell has always made himself available to help when I encountered challenges with research. He is a pleasure to be around and has a good sense of humor in and outside of the lab. I am lucky to have had the opportunity to work with him.

Abstract

Touch Amplification for Human Computer Interaction

by

Harald Schäfer

This thesis proposes a unique approach to haptic feedback, based on a hand-worn electronic device that amplifies the sense of touch. By capturing and reproducing touch elicited vibrations in real time, the feeling of otherwise natural finger-object interactions can be altered, while preserving temporal and spectral properties of the signal that are unique for every interaction and thus impossible to display without sensing and processing in real time. In order to shed light on the physical mechanisms through which such a device can operate, this thesis undertook an empirical investigation of the propagation of touch elicited mechanical vibrations (elastic waves) in the finger, and their dependence on the spatial pathway and frequency of excitation. Next, the thesis proposes a novel touch amplification system informed by these results, and addresses factors affecting the performance of the device, including the stability of the system at high gain levels. The results suggest promising applications in augmented reality and human-computer interaction.

Nomenclature

Chapter 2

$\vec{A}_p(f)$ The frequency domain acceleration vector at location p, $\vec{A}_p(f) = \mathscr{F}\{\vec{a}_p(t)\}$

$\vec{a}_p(t)$ The acceleration vector, $\vec{a}_p(t) = (a_{p,x}\ a_{p,y}\ a_{p,z})^\top$, measured at the location p

$A_m(f)$ The Euclidean norm of the frequency domain acceleration vector measured at location m

$A_{plate}(f)$ The Euclidean norm of the frequency domain acceleration vector measured at the plate

$H_m(f)$ The magnitude transfer function from the plate to location m

Chapter 3

A The digital amplification in the touch amplification device

E The energy of the signal received by the accelerometer during stability tests

f_0 The size of the frequency shift in the frequency shifting algorithm

$G(s)$ Transfer function that represents algorithms in the microcontroller

$H(s)$ Physical path from actuator to accelerometer, includes the effects of actuator's frequency response

$k(t)$ The Hilbert transformer used in the single sideband modulation algorithm

$L(s)$ The open-loop transfer function of the touch amplification system defined as $G(s)H(s)$

P The threshold used to determine stability during stability tests

s_0 The size of the frequency shift expressed as $s_0 = e^{j2\pi f_0}$

$U(s)$ The external touch input for the touch amplification system

$X(s)$ The signal read in by the accelerometer of the touch amplfication device

$x(t)$ The input of the single sideband modulation algorithm

$x_{ssbm}(t)$ The output of the single sideband modulation algorithm

$Y_{acc}(s)$ The output touch amplification device as measured at the accelerometer

$Y_{act}(s)$ The output touch amplification device as measured at the actuator

Contents

Abstract **v**

1 Introduction **1**
1.1 Background 2
1.2 Proposed Approach and Contributions 5

2 Transfer Properties of Touch Elicited Waves: Effect of Posture and Contact Conditions **7**
2.1 Introduction 10
2.2 Methods 12
2.3 Results 17
2.4 Conclusions 20

3 The Design of a Touch Amplification Device **22**
3.1 Introduction 24
3.2 Design 25
3.3 System Model and Stability 27
3.4 Feedback Suppression 29
3.5 Stability Assessment: Empirical Method 35
3.6 Results 35
3.7 Discussion 36
3.8 Applications 37

4 Conclusions **41**
4.1 Contributions 42
4.2 Discussion and Future Implications 43

A Microcontroller Code **45**

Bibliography **57**

Chapter 1

Introduction

Haptics involves the engineering of devices that can reproduce touch experiences in much the same way that a graphical display is able to reproduce visual experiences. The former arise from mechanical and thermal signals felt by the skin and the latter from optical signals captured by the eye. As a field, haptics is growing rapidly, and interest in the development of haptic interfaces is increasing, leading to activity in research and consumer markets. Haptic feedback can increase the realism and efficiency of human-computer interactions [6], but progress in their development has been slow due to the inherent challenges in their design. The engineering challenges involved in designing haptic displays arise from the complex, high-dimensional mechanical signals that are routinely felt by the skin when we touch objects, and the sensitive dependency of these signals on movements of the body – what we feel is affected greatly by how we touch an object.

The goal of this research is to realize a **wearable electronic interface for haptic augmented reality** that will provide haptic feedback to the hand when users are touching real surfaces, in order to simulate the perceptual experience of touching different objects or materials. In order to render touch feedback that is more realistic than

can be achieved with synthetic signals, we will design touch feedback by electronically capturing mechanical signals, in the form of contact-dependent vibrations, that are felt by the hand, in real time, and by modifying and amplifying those signals in order to manipulate what the hand feels. The operating principle is based on the notion of touch amplification - the device will be designed to amplify touch sensations for the hand in the same way that a hearing aid is able to amplifying sound for the ear.

As one illustrative application, imagine that a user is able to project a virtual keyboard onto a desk or table (figure 1.1). A wearable touch amplification device captures mechanical signals felt by the fingers as the surface is tapped. When the finger taps an active area of the virtual keyboard (such as a key), the mechanical signals felt by the finger are selectively amplified and filtered in order to produce the sensation that the user is tapping a physical key, eliciting a palpable "click" sensation. This type of scenario is more fully described in Chapter 3 of this thesis.

1.1 Background

Touch amplification involves electronically capturing and amplifying mechanical signals that are felt when an individual is touching an object. This concept has previously been explored by Chartier et al. [8], who explored the basics of touch amplification and feedback dynamics. Yao et al. [32] investigated the uses and benefits of a tool that amplifies the sense of touch. The authors developed a surgical instrument that could help users find otherwise undetectable lesions human tissue. The idea of a wearable haptic device that can augment and amplify the sense of touch for a variety of different applications has been suggested and tested by Maeda et al. [19, 20]. Their *HapticAid* device consists of a haptic actuator worn on the wrist and an accelerometer on the index finger. The device has many proposed applications including touch augmentation and sharing haptic

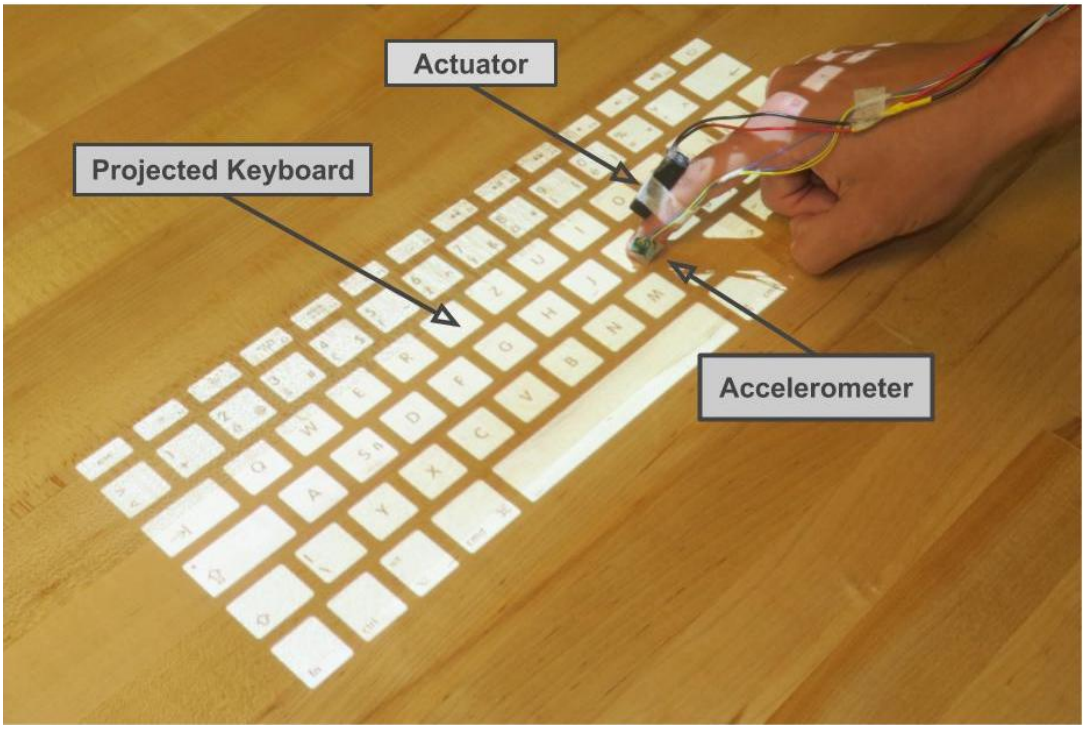

Figure 1.1: A virtual keyboard application motivating the research presented in this thesis. The virtual keyboard is projected onto an arbitrary surface. The touch amplification device works in conjunction with a motion capture system (not shown) in order to sense the position of the finger allowing the touch amplification system to dynamically amplify finger contact sensations when a virtual key is pressed (without affecting non-key areas), eliciting the perceptual sense of depressing a physical key. Amplification is achieved by sensing transient mechanical signals (vibrations) felt by the finger by means of a MEMS accelerometer, and reproducing a modified version of these signals via a finger-worn actuator.

sensations with others.

Existing haptic interfaces can generally be classified according to the mechanical simplifications that they must adopt in order to make their engineering practical. One category, surface haptic devices, consists of devices that have a usually flat surface with which the user can interact. This surface can provide haptic feedback with electromechanical actuators [4, 13, 25] or electrocutaneous displays [2]. Another category consists of devices that require users to interact by means of a handheld tool, which returns forces to the hand in response to movements in a virtual environment. Such devices generally

employ electromechanical actuators (typically DC motors) for haptic feedback [9, 12, 17]. Both approaches introduce mechanical constraints that greatly limit how users are able to interact. A wearable device that might provide feedback to the hand during unconstrained interactions would be preferable, but research on devices such as whole hand exoskeletons has failed to advance, due to the inherent difficulty posed in matching the kinematic complexity, range of forces, speed, and precision of the hand.

The design of a haptic interface requires a basic understanding of tactile sensory abilities, in much the same way that designing a good loudspeaker requires a basic understanding of the auditory sense. The skin is highly innervated with mechanosensory cells – specialized end organs of the nervous system that respond to mechanical signals for touch perception [16, 15]. In glabrous skin (the hairless skin on the palmar face of the hands and feet), there are four main types of mechanosensory cells. Two of these, the Merkel endings and Ruffini-like endings, are only sensitive to static deformations, or low frequency ($< 5Hz$) mechanical signals. The remaining two, Meissner and Pacinian corpuscles, are sensitive to mechanical signals in a broad frequency range, spanning at least 5 to 500 Hz. These provide us with the ability to sense mechanical changes in contact, mechanical vibrations in the range of touch perception (called *vibrotactile signals*) and similar effects. Because vibrations can be readily reproduced using low cost hardware, this method of stimulating the sense of touch is widely used in consumer devices and is also used in the device presented in Chapter 3.

Designing effective haptic display methods that use vibration excited in the skin requires a good understanding of how vibrotactile waves propagate through the finger. Although previous research has investigated this [28, 21], less research has been constructed on the influence of finger positions and contact conditions on the wave propagation in the finger. As a wearable haptic device will be used in a dynamic environment where the finger moves and interacts with surfaces and objects, it is important to understand how

changes in the finger conditions affect vibrations in the finger.

In a touch amplification device on the finger the signal from the actuator feeds back into the accelerometer, which means unstable feedback can limit the usable gain for such a device. Such a situation is frequently encountered in audio devices, such as public address systems and hearing aids. Those devices have a microphone that records acoustic signals and plays those sounds on a loudspeaker close to the microphone. This can create a feedback loop as the sound from the loudspeaker feeds back into the microphone. Under some conditions this will cause instability (also called howling or the Larsen effect) [30]. An important element of designing these devices is avoiding this type of instability. To make an effective touch amplification device, a high maximum usable gain is desirable and feedback suppression methods will likely be necessary. Many of these algorithms exist ranging from simple [7, 27, 24, 33] to more complex [5, 22, 14].

1.2 Proposed Approach and Contributions

The goal of this research is to realize a wearable electronic interface for haptic augmented reality. This device will provide haptic feedback to the hand, in the form of touch-dependent vibrations. It will do this by electronically capturing mechanical correlates of touch contact – i.e. contact-dependent vibrations – in real time. By modifying and amplifying those signals, and displaying them concurrently with a user's touch interaction, it seeks to manipulate (amplify or modify) what the hand feels during otherwise natural touch interactions.

In order to address the challenges of realizing such a touch amplification display, this thesis contributes in two main areas. First, in Chapter 2, it contributes to the state of knowledge about characteristics of touch elicited vibration propagation in the hand, a subject that has received little prior attention. Through several experiments,

my colleagues and I mapped the spatial and frequency distribution of touch elicited mechanical signals in the finger. The results provide valuable guidelines for the design of electronic interfaces that might reproduce these signals. Observations in Chapter 2 indicate that contact forces of the finger consistently influence that attenuation of elastic waves (vibrations) propagating in the finger. In contrast, the influence of finger posture was more challenging to understand.

Chapter 3 of this thesis draws on the knowledge obtained through the experiments of Chapter 2 in order to guide the design of a wearable haptic device, the first of its kind, for stably amplifying touch sensations in the finger in real time. First, a wearable touch amplification system is provided, including electronic analog and digital signal processing components that make it possible to implement a vibration amplification scheme in real time, under parametric control from a personal computer that has mapped the 3D physical environment (for example, the desk and key locations, in the example recited above). A fundamental limitation affecting the dynamic range of the resulting system arises from feedback (in)stability, which limits the feasible dynamic range of gains that can be used. The remainder of Chapter 3 proposes and evaluates several methods for increasing the range of usable gains. By adopting a frequency shifting method that has been proposed in prior literature on feedback suppression, it is shown that it is possible to increase the usable gain by approximately 10 dB, ensuring crisp haptic effects can be provided.

Chapter 2

Transfer Properties of Touch Elicited Waves: Effect of Posture and Contact Conditions

Attribution and Permissions

The content of chapter 2 is from the following reference [26]:

H. Schäfer, Y. Shao, Z. Wells and Y. Visell, "Transfer Properties of Touch Elicited Waves: Effect of Posture and Contact Conditions". Proc. of IEEE World Haptics Conference, 2017 (Accepted).

It is reproduced here with the permission of the IEEE. Harald Schäfer conceived the work, implemented the experimental system, ran experiments, drafted the manuscript, and prepared figures.

Preface to Chapter 2: Significance for the Thesis

Chapter 2 empirically investigates the propagation of touch elicited vibrations, or elastic waves, in the finger and their dependence on spatial location and frequency. The chapter also addresses how the patterns of propagation in space and frequency are influenced by the contact conditions and posture of the finger. The results will serve as crucial background knowledge when designing the touch amplification device in Chapter 3.

Abstract

During haptic interaction with touched objects, contact with the skin elicits mechanical signals that propagate rapidly to distances removed from the location of contact. Prior research has shown that these touch elicited mechanical signals travel predominantly as waves, and during manual touch, reach distances spanning the entire hand. While the structure in these signals is well preserved across distance, it is unknown how the propagation of these signals from the contact locus to other areas of the hand or finger depend on posture or contact conditions. To address this, we measured empirical transfer functions from a contacting plate that stimulated the fingertip to other sites on the finger, and analyzed the dependence of the corresponding frequency domain transfer functions on location, posture, and contact forces. The results suggest that the frequency and spatial dependence of these transfer functions varied consistently, and encoded contact conditions and relative contact location. Greatest variation was observed in the low or high frequency ranges of vibrotactile sensation, and at large distances from the contact surface. In contrast, mechanical information in the frequency range from 100 to 200 Hz was well preserved at large distances, and across conditions, indicating that tactile information in this frequency range is transmitted to other finger locations in a manner that is relatively invariant to the conditions and location of touch contact. The results may refine current understanding of the biomechanics of cutaneous wave propagation in the hand, may hold implications for understanding information content in touch-related cutaneous waves, and could inform the design of tactile displays worn on the skin.

2.1 Introduction

Despite decades of research in haptics and interest in haptic displays that can simulate natural touch experiences, our understanding of the mechanical signals that are felt by the body during touch contact with real objects or surfaces is incomplete. This can be attributed to the distributed nature of the skin, the complexity of its biomechanics and contact mechanics, and the multiple time- and length-scales and physical regimes that are involved. A fuller understanding of biomechanics can aid our understanding of touch sensation and perception, elucidate biological specializations of the haptic system, and inform the design of future haptic interfaces.

A longstanding goal of haptic engineering has been to design wearable displays that stimulate distributed areas of the skin, and that yield realistic touch sensations. However, an often overlooked challenge to realizing such an objective lies with the difficulty of predicting how the skin would respond to touch contact, and how the distributed response of the skin is related to contact parameters, tissue properties, or the posture of the hand itself. Stated simply, it is currently difficult to understand how or what the skin feels, it depends on what we touch, how we touch and how the hand is employed. An increased understanding of such factors would greatly aid the engineering of rendering algorithms and haptic display hardware, including wearable devices that are in sustained or distributed contact with the skin.

Recent research has demonstrated that touch elicited waves can propagate far away from their source [28, 18, 11, 21, 29], and that, during natural interactions with ordinary objects, mechanical signals originating at the finger typically travel distances spanning the whole hand at levels that are physiologically and perceptually relevant [18]. This yields remote mechanical signals that preserve spatiotemporal signatures of skin-object contact, properties of the surfaces that are touched, and the type of touch contact that

is involved [11, 28]. Due to the differences between the transmission pathways that are involved, and attenuation and frequency-dependent alterations that result, different parts of the limb feel distinct signals in response to the same stimulus [21, 28, 29], depending on distance from the contact locus, and perhaps on other factors, such as the pose of the limb. Such dependencies might, for example, provide a means of inferring contact location or related conditions from differences between remote mechanical signatures of touch. Despite suggestive findings in the aforementioned studies, it is not generally known how the transfer-dependent alteration of touch-elicited waves might reflect contact distance, conditions at the fingertip, or the posture of the hand and fingers.

To address this, we measured empirical frequency domain transfer functions from a contacting surface that supplied controlled vibrations to the fingertip to six locations on the finger, by comparing the acceleration of the contact surface with that of the skin at the remote locations, and analyzing the results. By manipulating hand postures and contact force levels in the experiment, we were able to demonstrate that posture, contact conditions, and distance were reflected in the mechanical filtering of cutaneous waves, in frequency and spatially dependent ways.

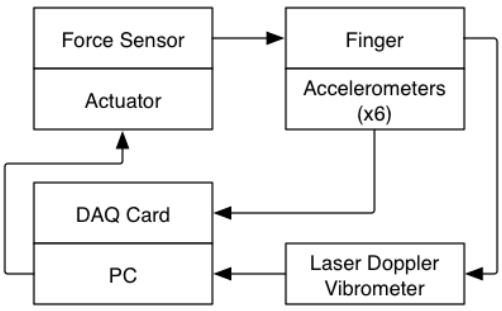

Figure 2.1: Schematic representation of the apparatus used in the experiments.

2.2 Methods

We used contact and non-contact methods in order to measure the transfer function governing the propagation of cutaneous waves from the fingertip to six different locations on the finger, and varied the hand posture and contact force in order to assess the role of contact conditions, posture, and distance in transforming remotely sensed contact signals at different frequencies.

2.2.1 Apparatus

To stimulate the fingertip and record surface vibrations, we supplied controlled vibrations to the fingertip via a rigid aluminum plate coupled to a voice coil actuator-based haptic display developed in our earlier research [31]. This device is capable of producing up to 37 N of static force, 90 N of transient force, and has a mostly flat frequency response up to at least 500 Hz. Because we directly measured the motion of the plate for comparison to the motion of the skin, and compute transfer functions as quotients of these factors (Eq. 2.1), our analysis does not depend on the frequency response of the actuating system. The actuator was driven by a custom current amplifier and a motion controller (DMC-4123, Galil Motion Control, Rocklin, USA) operating with a sample frequency of 7000 Hz.

To record vibrations of the skin, we used an array of skin-mounted miniature accelerometers (Model ADXL335, Analog Devices Inc., Norwood, MA) on custom thin PCB packages (combined mass 0.6 grams per sensor), and employed a non-contact Laser Doppler Vibrometer LDV (Polytec PDV 100, Irvine, CA) in order to ensure that the skin-mounted accelerometers did not affect the measured vibrations. The accelerometers captured acceleration in three Cartesian axes (X, Y, Z) and had a frequency bandwidth covering the entire measurement range (0 to 1600 Hz in X and Y; 0 to 550 Hz in Z). Dur-

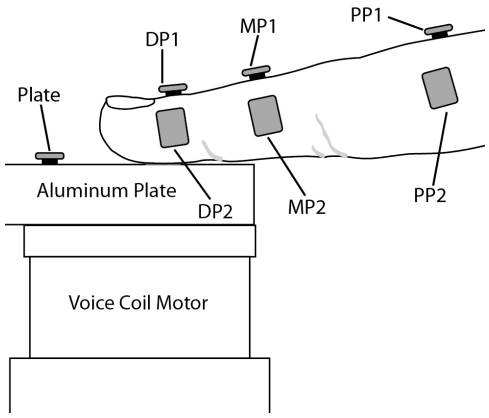

Figure 2.2: Anatomical positions of 6 accelerometers distributed on the index finger. On each segment of the finger, including Distal phalanx (DP), Middle phalanx (MP) and Proximal phalanx (PP), one accelerometer was positioned on the dorsal side and one on the radial side of the finger. One additional accelerometer is attached to the aluminum contact plate in order to capture vibrations applied to the fingertip.

ing one experiment, a force sensor (Model LLB130, Futek Inc., Irvine, CA) was mounted on the aluminum plate to capture finger-surface contact forces between the finger and the stimulating plate. The sensor data was captured via a data acquisition card (Model PCIE-6321, National Instruments, Austin, TX), and both the LDV and accelerometer signals were subsequently processed using a personal computer, which also commanded the actuator during the experiments (Figure 2.1). The sensing apparatus was mounted on a pneumatically isolated optical bench, while a separate structure was used to position the actuator, isolating it from both the hand and the sensors. Optics mounted on the table directed the laser beam to specified measurement locations on the skin or apparatus.

Six accelerometers were attached to the index finger using lightweight cosmetic glue (Pros-Aide, FXWarehouse, Philadelphia, PA), while one was firmly glued to the aluminum stimulating plate, near the location of finger contact (Figure 2.2). The finger-worn accelerometers were placed on the dorsal and radial side of each of the distal, middle and proximal phalanges, with one sensor on each of the dorsal and radial side (Figure

2.2).

During validation trials with the LDV, the stand off distance of the laser to the finger skin was set to 1062 mm, ensuring high resolution and sensitivity. The LDV low pass filter was set to 5 k Hz, while the high pass filter was disabled. Based on preliminary testing, we used a velocity range setting of 500 mm/s for signals below 80 Hz and 100 mm/s for higher frequency signals.

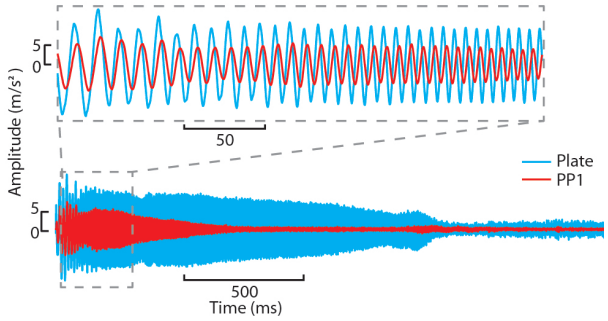

Figure 2.3: Example recording of accelerometers mounted on the aluminum plate and the dorsal surface of the] proximal phalanx (z-axis signal only). The displayed stimulus is a 60-800 Hz chirp with duration 2.3 seconds.

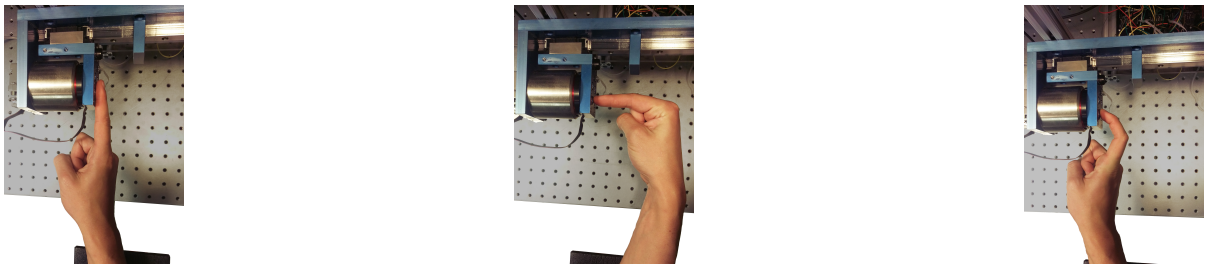

Figure 2.4: The experiments investigated the effect of three different hand postures on the mechanical filtering of touch-elicited waves: Posture A (left), posture B (middle), and posture C (right).

2.2.2 Measurement Procedure

In a first experiment, we investigated the transfer properties of the finger for three different hand postures, while in a second experiment we studied the same transfer prop-

erties for two different values of the contact force between the finger and the plate.

During the experiments, we measured skin and plate accelerations, the index finger contacted the plate with the hand held in one of three different postures (Fig. 2.4). In posture A, the index finger contacted the plate parallel to the latter, with the metacarpophalangeal (MCP) joint at 180 degrees. In posture B, the index finger contacted the plate normal (orthogonal) to the latter, with the MCP joint at 90 degrees. In posture C, the distal interphalangeal (DIP) joint was maintained at 30 degrees, the proximal interphalangeal (PIP) joint was held at 45 degrees, and the distal phalanx contacted the plate at an angle of 45 degrees in the median plane of the finger.

In Experiment 1, a constant force level of 4 Newtons was maintained between the contact plate and the fingertip. Acceleration data (Fig. 2.3) was collected as the plate was driven with sinusoidal sweeps that varied in frequency from 20 to 500 Hz. We employed several overlapping frequency sweeps and combined the results to ensure high resolution at all frequencies. This was repeated 20 times for each of 3 postures and each of three participants (3 males, 21 to 26 years old), yielding data for a total of 180 transfer function measurements. The Human Subjects Institutional Review Board of the authors' institution approved the procedures used in the study, and written consent was obtained from the participants.

In Experiment 2, the force sensor was introduced between the plate and finger in order to quantify the mean contact force. Using visual feedback from a force indicator, participants maintained light force (4 N) or high force (15 N). This was repeated eight times for each force level and each posture for each of two different participants (2 males, age 25 and 26), yielding a total of 96 transfer function measurements.

In order to ensure that contact from the skin-mounted accelerometers did not affect the measured signals, we repeated the measurements from Experiment 1 for posture A using the LDV sensor. The results were highly similar to those obtained with the

accelerometers, within ±1 dB across most of the frequency range, and ±2 dB across the entire range, indicating little effect of the accelerometer on measured transfer properties. In addition, because our analysis methodology involves a quotient of frequency responses measured at the plate accelerometer and finger accelerometers, any intrinsic gain or dynamics in the accelerometer was eliminated in our estimate.

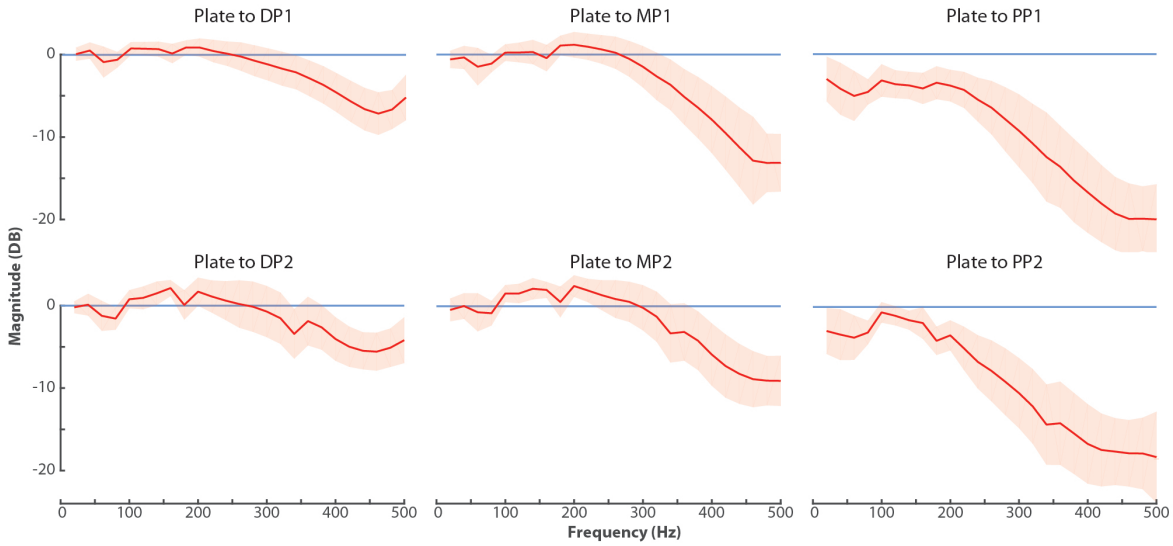

Figure 2.5: The transfer functions from 180 trials (3 different postures, 3 different users and 20 trials per user from experiment 1) from the stimulating plate to each of the 6 positions on the finger. The blue line represents the unit gain line. The red line represents the average. The shaded area represents the standard deviation.

2.2.3 Analysis

The measurements consisted of time-varying acceleration vectors $\vec{a}_p(t)$ at each of seven measurement locations, i.e. for $p = \mathsf{Plate}, \mathsf{DP1}, \mathsf{DP2}, \mathsf{MP1}, \mathsf{MP2}, \mathsf{PP1}, \mathsf{PP2}$, see Figure 2.2. At each instant, $\vec{a}_p(t) = (a_{p,x}\ a_{p,y}\ a_{p,z})^\top$ is the vector acceleration at the measurement point in the coordinate frame of the measurement location p. Using the discrete fourier transform $\mathscr{F}\{\cdot\}$, we computed frequency domain (vector) accelerations $\vec{A}_p(f) = \mathscr{F}\{\vec{a}_p(t)\}$, and computed the instantaneous scalar magnitude spectrum,

$A_p(f) = ||\vec{A}_p(f)||$, where $||\cdot||$ is the vector Euclidean norm. Using scalar acceleration values allowed us to consistently combine acceleration values between sensors independent of their orientations on the skin or plate. We resampled the frequency variable in 20 Hz steps for further analysis.

We computed (magnitude) transfer functions $H_m(f)$ from the plate location to each measurement location m on the finger, $m = \mathsf{DP1}, \mathsf{DP2}, \mathsf{MP1}, \mathsf{MP2}, \mathsf{PP1}, \mathsf{PP2}$, via the quotient.

$$H_m(f) = A_m(f)/A_{\mathsf{plate}}(f) \tag{2.1}$$

For each experimental trial, condition, and subject, we obtained six such transfer functions, one for each location m on the finger. For each condition and location, we computed summary statistics at each frequency, as reported below.

2.3 Results

Experiment 1 yielded 180 transfer function measurements describing the frequency-dependence and hand posture dependence of the transformation of signals from the contacting surface to six locations on the finger. The results (combining data in all postures) are summarized in Figure 2.5. The transfer function magnitudes were largest in the 100 to 300 Hz range, indicating that signal amplitude was well preserved at these frequencies, and in the regions of the distal and middle phalanges, was selectively amplified, due to tissue mechanics, as observed in prior research [21], and analogous to resonances observed in whole arm vibration measurements [1]. Amplification was greatest in the middle phalanx, indicating that the surface of the skin experienced the largest acceleration in these locations, approximately 0 to 4 dB greater than at the contacting surface. There are several peaks and notches in the transfer function at various frequencies, and

these proved consistent between trials and postures of the hand, and were, in some cases, qualitatively preserved from location to location, revealing a nuanced pattern of mechanical filtering. At frequencies greater than 300 Hz, the transfer function magnitude decreased at all locations, indicating that high frequency signals were most attenuated when traveling to large distances in the finger, except at the largest frequencies, approaching 500 Hz, where attenuation decreased (and in some conditions reversed). This attenuation was most pronounced at locations on the proximal phalanx, although even here, the amount of attenuation (15 to 25 dB) was small enough that it could preserve signals at physiologically and perceptually relevant levels.

Experiment 1 also yielded transfer functions to locations on the finger when the hand was in one of three postures, A, B, or C (Figure 2.6). From the results, posture-dependent differences between transfer functions were most pronounced in the middle and proximal phalanges. At low frequencies, posture B transmitted tactile signals much more efficiently, with more than 5 dB greater gain in the proximal phalanx, than postures A or B did, perhaps because of the normal orientation of the finger with respect to the plate. At high frequencies, there was little difference in stimulus propagation to the distal phalanx across the entire frequency range, indicating surprisingly little dependence of the transfer functions on the contact orientation or degree of flexion of the fingers. In short, the distal part of the finger received similar signals irrespective of the orientation of the finger. This indicated that hand posture might affect the transmission of tactile signals across large distances in the finger, that the effects remained most pronounced at low frequencies and large distances, and that these low frequency differences in tactile transmission had an effect that was about as large as that due to transmission to the base of the finger (i.e., near the MCP joint).

Experiment 2 yielded 96 transfer functions describing the frequency-dependence and force-dependence of transformation of signals from the contacting surface to locations on

the finger (Figure 2.7). At low frequencies, below about 250 Hz, there was little difference between signal transmission in the presence of low vs. high contact forces. In contrast, at low contact force levels, there was more attenuation at high frequencies. This held for all locations on all phalanges. The effect was most pronounced at greater distances from the contact location, indicating that light touch may preserve less the transmission of high frequency content in tactile signals during transmission to large distances in the finger.

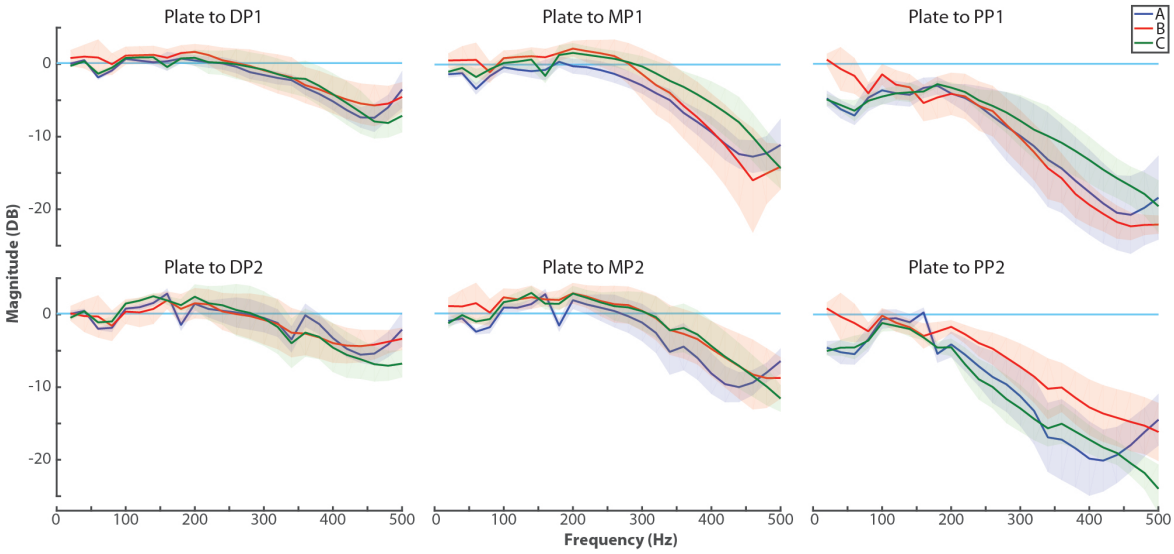

Figure 2.6: Transfer functions from the contact surface to six locations on the finger, as obtained in Experiment 1, for three different hand postures. Blue, red, and green lines indicate postures A, B, and C. Cyan colored horizontal line: unity gain (0 dB). Shaded area: 1 standard deviation.

A further examination of the variability in this data, exemplified through the standard deviation in the magnitude transfer functions from both experiments 1 and 2 (Figures 2.5, 2.6 and 2.7), reveals consistently greater variability at high frequencies, indicating that the extent of transmission of high frequency tactile signals to distributed areas of the finger could readily change between conditions or trials. This could be because of the shorter wavelength of these signals, which can make them more sensitive to small changes in the transmission path from the contact surface to the measurement location. One can

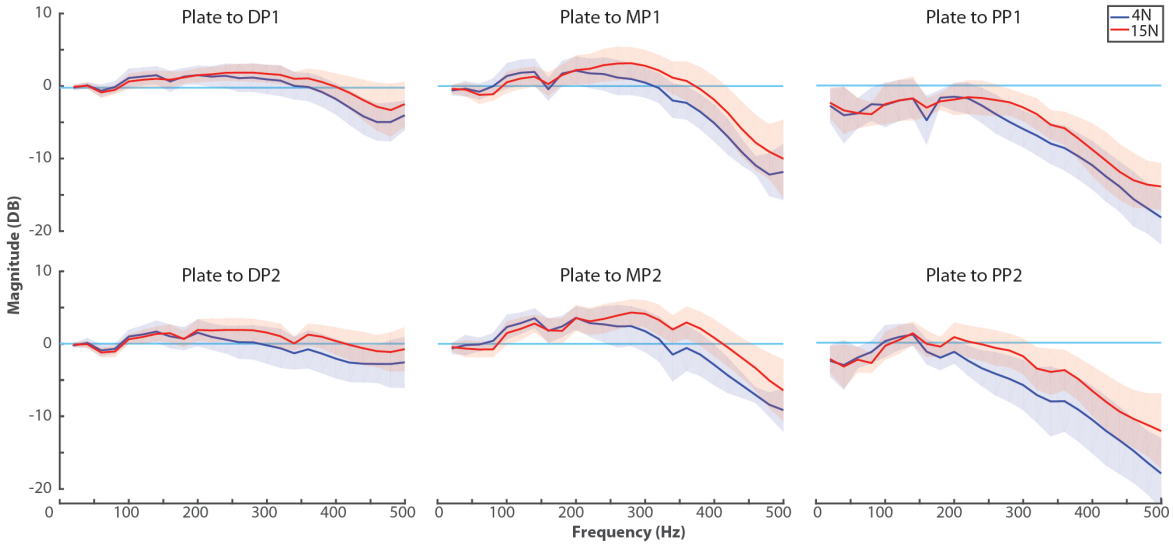

Figure 2.7: Transfer functions from the contact surface to six locations on the finger, as obtained in Experiment 2, for low and high contact force levels. Red line and blue lines correspond to high force (15 N) and low force (4 N) conditions respectively. Cyan colored horizontal line: unity gain (0 dB). Shaded area: 1 standard deviation.

also observe that the standard deviation is largest in the middle and proximal phalanges, perhaps because the longer signal path may result in larger variability in impedance and geometry.

2.4 Conclusions

In this study, we measured empirical frequency domain transfer functions from the locus of contact between the finger and a contact surface, to an array of sites on the finger. The results revealed systematic variations in the transmission of tactile signals, depending on contact force, frequency range examined, and spatial locations considered. The differences were preserved across many trials, indicating that differences in tactile transmission in the finger could encode contact interactions of the finger. Greatest variations in these signals was observed at large distances, and at frequencies that were near the low or high end of the tactile frequency range. In contrast, we observed relatively stable

responses at intermediate frequencies, from about 100 to 200 Hz, across all conditions.

The data suggests several possible perceptual cues that could be explored in future research. For example, the ratio of low to high frequency signal amplitude modification decreased systematically moving proximally on the finger, indicating that, irrespective of the source signal content, an observer comparing the tactile transmission of low vs. high frequency signal components could use their ratio to estimate the distance to, and perhaps location of, a tactile stimulus on the skin.

In summary, these results may refine current understanding of biomechanical response in the skin, by illustrating the dependence of cutaneous wave transmission on the posture and contact conditions of the hand, by revealing the extent and type of variability in signal transmission in different frequency bands, and by demonstrating the variation in tactile transmission between regions of the finger.

Chapter 3

The Design of a Touch Amplification Device

Permissions and Attributions

The content of Chapter 3 is a work in progress by the author in preparation for submission as a future publication. It is reproduced here with the permission of UCSB.

Preface to Chapter 3: Significance for the Thesis

Chapter 3 describes the design of a touch amplification device based on capturing and parametrically altering and reproducing touch elicited vibrations in the finger. The chapter presents a novel hardware platform, with processing that can be dynamically altered through parametric signal processing algorithms implemented on a microcontroller. A fundamental limitation on the dynamic range of haptic effects that can be provided through such a device consists of the presence of feedback induced instabilities. In order to address these, several algorithms are proposed for feedback suppression, and demon-

strate that one of these – a frequency shifting method – is able to increase the stable range of gains of the system by approximately 10 dB, as determined through experiments, increasing the feasible palette of haptic effects with little additional computational cost.

3.1 Introduction

A touch amplification device based on capturing and parametrically altering and reproducing touch elicited vibrations in the finger has promising applications. Such a device can change the feeling of interactions with surfaces and objects. The work presented here describes the design of a generic touch amplification system with a versatile software framework that can be configured for many different applications (figures 3.1, 3.2). These applications include improving the capabilities of the human sense of touch, human-computer interfaces and augmented reality.

Here we will focus on overlaying real surfaces with virtual objects. One example of this is illustrated in figure 1.1. A virtual keyboard is projected onto a flat surface, with which the user can interact naturally. A motion capture system tracks the fingertip of index finger that wears the touch amplification device and based on its locations the parameters of the system are altered. If the finger is above or on a key the touch interactions are augmented providing haptic feedback to the user when sliding over or tapping on the virtual keys.

A touch amplification device requires an actuator and an accelerometer mounted close to each other (figure 3.1). When the actuator displays the signals that are measured on the accelerometer, the signal will feed back into the accelerometer and this can cause instability (figure 3.3). Acoustic systems that use microphones and speakers in a similar arrangement such as hearing aids and public address systems also encounter this issue. Suppressing feedback to prevent instability has been extensively researched for these acoustic systems, and methods used for acoustic systems will be experimented with for the touch amplification device to improve performance.

3.2 Design

Our device consists of an accelerometer and an actuator attached to the finger and is controlled by a digital control circuit that can be programmed for different types of real-time signal processing. The flexibility of a digital device will be a huge advantage when testing different feedback suppression methods and signal augmentation for augmented reality applications.

The accelerometer is mounted on the side of the distal phalanx of the index finger (figure 3.1). The accelerometer is set up to measure accelerations along the longitudinal axis of the finger.

Through informal testing it was determined that when the actuator is attached closer to the fingertip, the haptic feedback will be felt closer to the fingertip with which the user will interact with objects. This is desirable to make the touch amplification feel more natural so that the touch experience and the added vibrations of the actuator are felt in the same location. Unfortunately, the closer the actuator is mounted to the accelerometer, the less usable gain the device will have. This is discussed in more detail later. The actuator is too large and heavy to be mounted on the distal phalanx, so we choose to mount the actuator on the back of the proximal or intermediate phalanx.

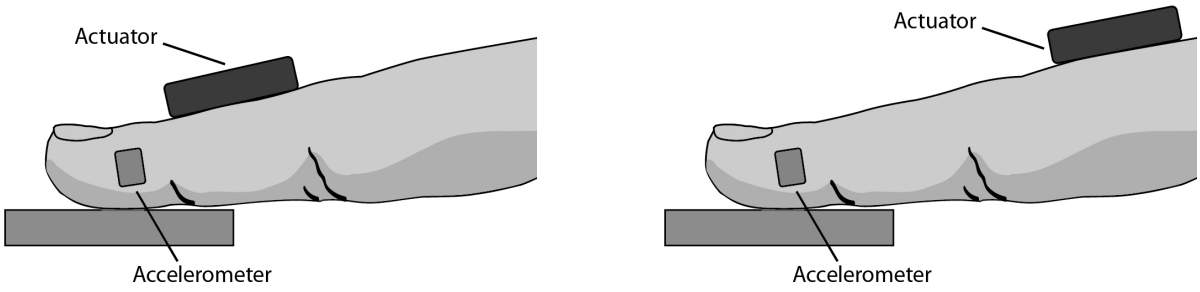

Figure 3.1: Two of the configurations used for the touch amplification device

3.2.1 Hardware Design

The touch amplification device uses an ESP8266 microcontroller for all on-board computation. The Wi-Fi capabilities of this chip allow wireless communication with a PC, and I2C is used to connect with the other embedded chips. The ESP8266 contains a 32-bit 80MHz CPU that is sufficiently fast for real time signal processing, and Wi-Fi connectivity at the 1600 Hz sample rate at which the device operates.

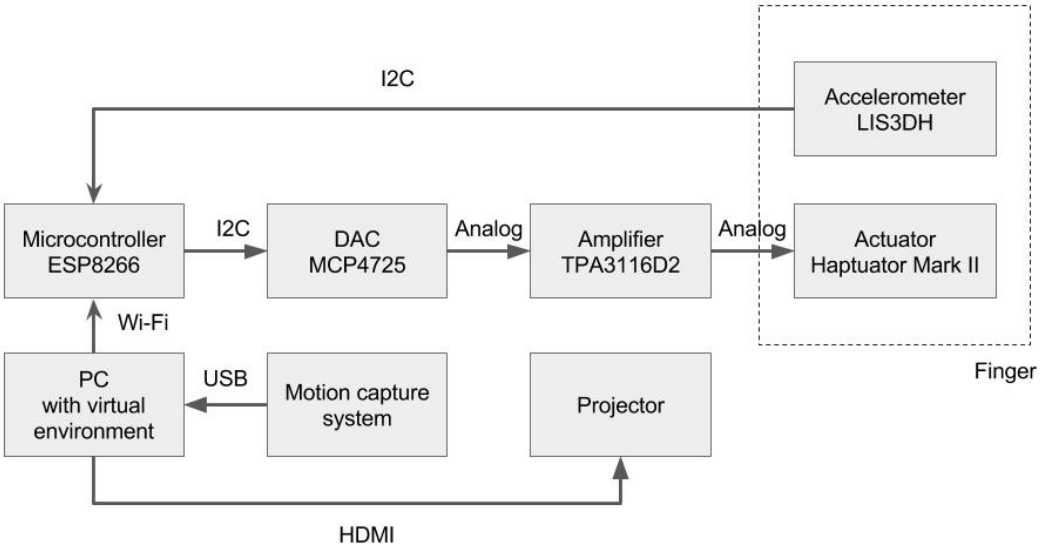

Figure 3.2: Diagram depicting the signal flow and all essential components of the touch amplification system.

Digitals accelerometers were chosen to measure the vibrations in the finger. The selected LIS3DH chips have a +/-16g detection range, a 1600 Hz sampling rate, and an I2C interface to connect to the microcontroller. Also on the I2C network is a digital to analog converter (MCP4725), that sends analog signals to the amplifier that drives the actuator.

The Haptuator Mark II from TactileLabs was the vibrotactile actuator of choice. This actuator has a high power output in a package small enough to be worn on the finger,

which makes it ideal for this application. It can display frequencies in the 100-900 Hz range and has a resonance around 150 Hz which can be seen in figure 3.7. This actuator can be powered with regular audio amplifiers. We opted for a low power ($20W$) audio amplifier that can easily drive it.

3.3 System Model and Stability

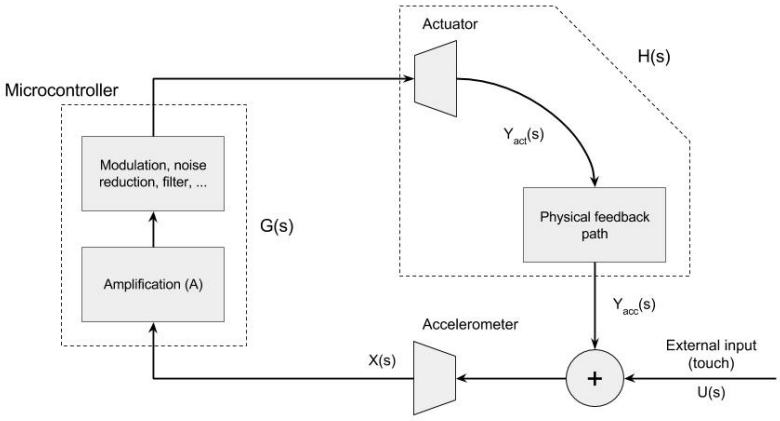

Figure 3.3: System diagram of touch amplification device. $G(s)$ is the forward path implemented on the microcontroller, where A is a simple gain factor. Y_{act} is the physical vibration signal measured at the actuator, and Y_{acc} is the physical vibration signal measured at the accelerometer. The accelerometer reads $X(s)$, which is the sum of the feedback signal Y_{acc} and the external touch elicited vibrations, $U(s)$. The actuator response and physical feedback path transfer functions are grouped together into $H(s)$.

We can represent the system as a simple continuous time linear feedback system (figure 3.3) in the Laplace domain (s-plane). The transfer function $G(s)$ represents all the digital filters, amplifiers and signal modifications on the microcontroller. In the simplest case, this is simply a gain: $G(s) = A$.

The physical path, which encompasses the actuator response and the transmission

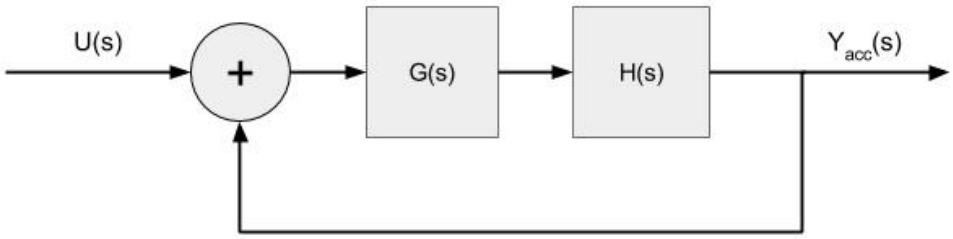

Figure 3.4: Simplified system diagram of the touch amplification device.

path through the finger from the actuator to the accelerometer, is defined as $H(s)$. The external input caused by touch interactions with the finger is defined as $U(s)$ and the signal that is read by the accelerometer is named $X(s)$.

If we consider $Y_{acc}(s)$, the vibrations at the accelerometer, to be the output and $U(s)$ to be the input, then the open loop transfer $L(s)$ becomes

$$L(s) = G(s)H(s) \tag{3.1}$$

The closed loop system (Fig. 3.4) is described by

$$Y_{acc}(s) = L(s)U(s) + L(s)Y_{acc}(s). \tag{3.2}$$

The transfer function becomes

$$\frac{Y_{act}(s)}{U(s)} = \frac{L(s)}{1 - L(s)} \ . \tag{3.3}$$

Assume $G(s)$ and $H(s)$ are stable. Because the actuator output is added to (not subtracted from) the input (Fig. 3.4), the Nyquist criterion for the closed loop stability

of the system takes the form

$$|L(s)| < 1 \quad \text{when} \quad \angle L(s) = 2\pi n \quad n = ..., -2, -1, 0, 1, 2... \tag{3.4}$$

The stability gain margin is given by the maximum magnitude of $1/L(s)$ at phase 2π, or in dB by $-20\log_{10}|L(s)|$, at phases $2\pi n$. This is the amount that the feedback gain of the system can be increased before the system becomes unstable. It represents a limitation on the feasible range of touch amplification. In the following sections, methods are explored for increasing the gain margin of the system.

3.4 Feedback Suppression

If the gain exceeds the gain margin, the system will become unstable. In general, we do not have a model of the system dynamics – in particular, $H(s)$ is not known and is very complex. It includes important contributions due to the propagation of mechanical signals in tissues of the finger, a continuum mechanical system, as presented in Chapter 2. Those results (Fig. 3.5) indicate that the attenuation of the physical path through the finger is small in the frequency range of interest. For example, in the 100-250 Hz frequency band, the attenuation is as low as -3 dB for an elastic wave propagating along the entire length of the index finger. This indicates that instability could occur first in this range, and that it might occur at low gain settings. It is also clear that the attenuation is larger when the distance traveled through the finger is longer, this indicates that placing the actuator further from the accelerometer, such as on the proximal phalanx (figure 3.1), can improve the stability of the system. However, it is preferable to be able to the mount the actuator closer to the fingertip – for example, on the intermediate phalanx. These factors indicate that to be able to achieve high amplification desirable for many applications, we

will need to use effective feedback suppression methods to prevent instability.

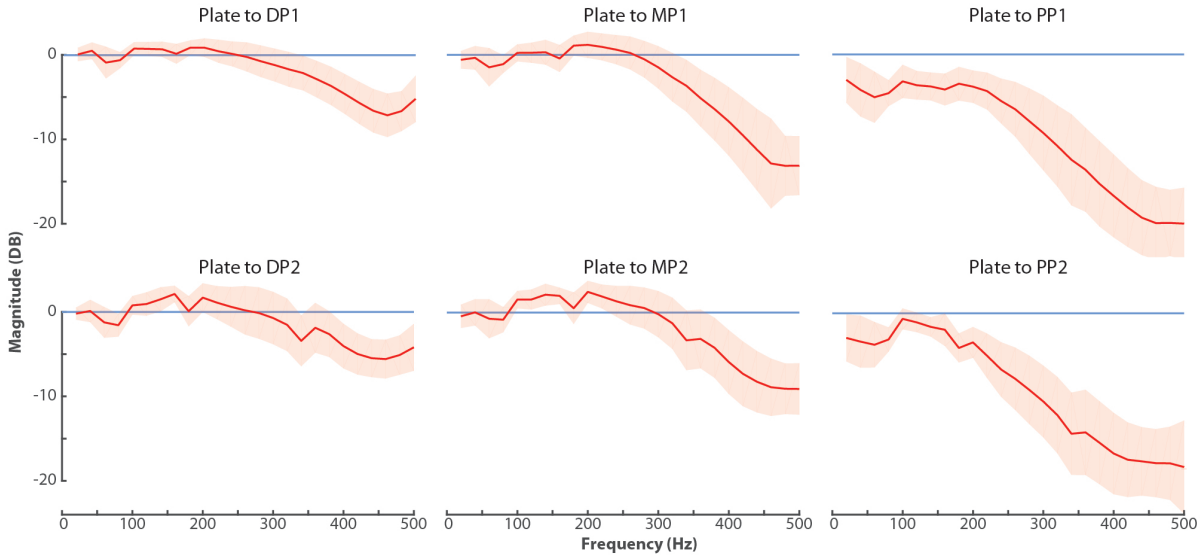

Figure 3.5: Transfer properties of touch elicited waves in the finger to different locations (Reproduced from figure 2.5).

Hearing aids and a variety of acoustic systems need similar feedback suppression algorithms to improve performance [7, 27, 24, 33, 5, 22, 14]. The most effective of these methods generally use adaptive filters to make a dynamic estimate of the feedback path and subtract it from the input from the accelerometer or microphone. The system diagram for such a setup is shown in figure 3.6. Unfortunately, those methods generally require a somewhat static and predictable feedback path. While the results of Chapter 2 do make clear some general trends in how vibrations propagate through the finger depending on conditions, there is still a large degree of uncertainty (standard deviation above 2dB). Additionally, we concluded that contact forces consistently influence the wave propagation in the finger. This means that when a user of the touch amplification device taps a surface, the feedback path is likely to change significantly during this interaction. Creating an adaptive filter that can accurately estimate the feedback path of the system in such a rapidly changing environment would be challenging.

In this thesis, simple methods explored for improving the feasible range of gains

without recourse to dynamic channel estimation. The methods include static filtering of the signal, to attenuate signal components that destabilize the system while leaving others, including frequency ranges to which users are sensitive, intact.

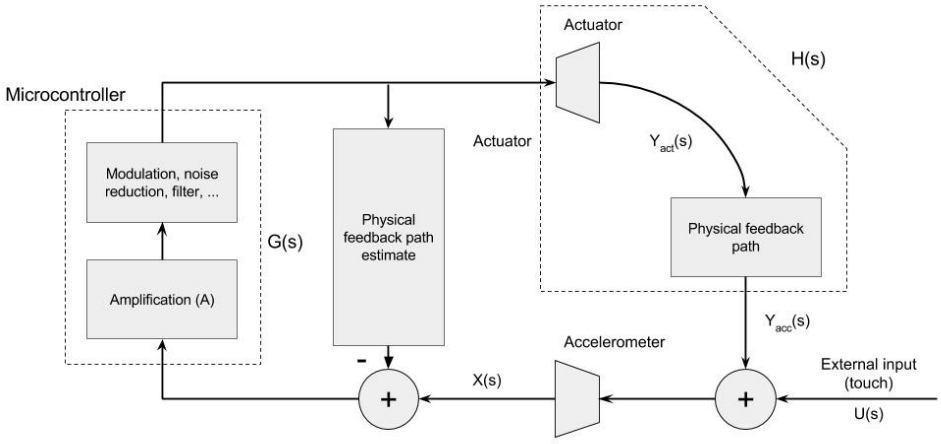

Figure 3.6: System diagram of the touch amplification device with an adaptive filter estimating the physical feedback path for the purposes of feedback suppression.

3.4.1 Actuator Compensation

The frequency response of the system can be greatly affected by the actuator dynamics. In our device, the actuator response is not flat 3.7, but possesses a resonant region in the 100 - 200 Hz range. This resonance causes a peak in $L(s)$, the open loop transfer function. Empirically, this contributes to an unstable mode of the closed loop system near that frequency. The same resonance also affects the frequency response of the system, creating an imbalance between frequency content presented to users, and affecting how it is perceived. To address this, we integrated digital filtering $F(s)$ in the loop gain $L(s)$ of the device, mitigating the effect of the actuator dynamics, increasing usable gain

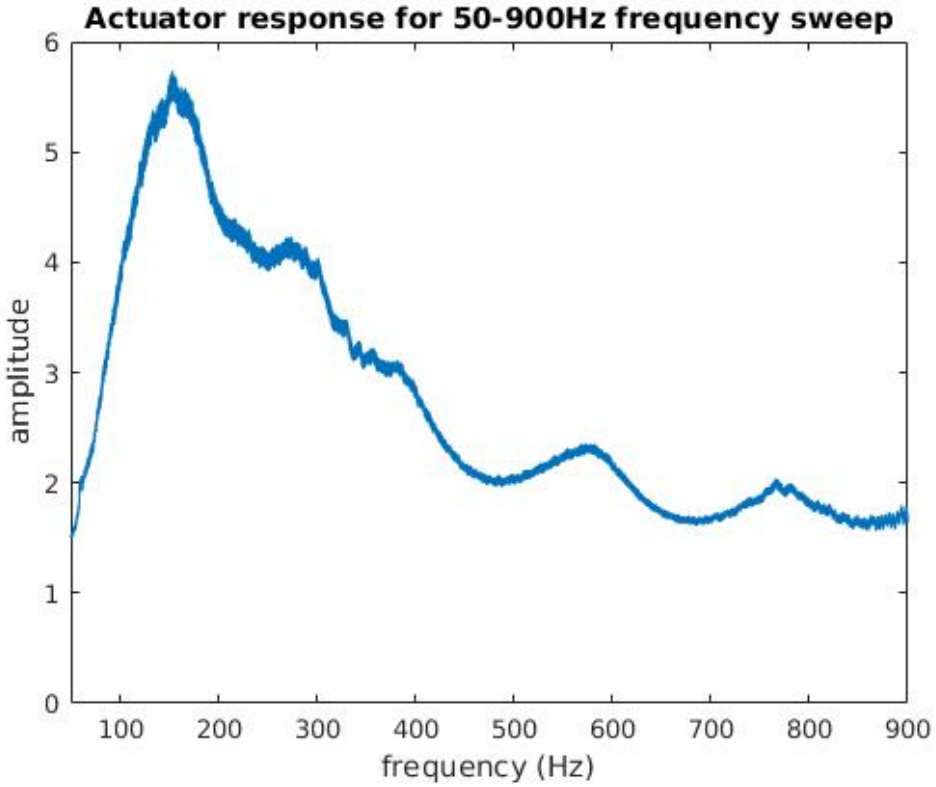

Figure 3.7: Actuator response of the actuator used in the touch amplification device. This response was measured with the actuator mounted on the intermediate phalanx of the finger.

and improving the perceptual transparency of the device. $L(s)$ was then given by

$$L(s) = AF(s)H(s) \tag{3.5}$$

From looking at the frequency response data of the actuator, $F(s)$ was chosen to be a 160 Hz high pass filter. Choosing a cutoff frequency right at the resonance attenuates the resonance and ensures a more flat response. The filter implemented was a 2nd order IIR filter designed with the butter-worth method.

3.4.2 Frequency Shifting

Frequency shifting is a commonly used method to suppress unstable feedback in acoustic systems [3, 27, 24]. This method is simple to implement and can provide positive results without requiring in-depth analysis of the feedback system. However, due to the high frequency sensitivity of human ears only a small frequency shift can be applied before the signal noticeably deteriorates (max 12 Hz recommended [30]). Fortunately, the low frequency resolution of the finger's mechanoreceptors [15] means the change in spectral characteristics are less important in haptic devices than in audio devices.

In our system we implement frequency shifting by using a single sideband modulation algorithm on the signal in the microcontroller that shifts the input signal with a fixed frequency f_0. The time-domain expression for this modulation, with $x(t)$ the signal to be modulated, is described as

$$x_{ssbm}(t) = x(t)\cos(2\pi f_0 t) - \big(k(t) * x(t)\big)\sin(2\pi f_0 t) \tag{3.6}$$

where $*$ is convolution, and $k(t_n)$ is a Hilbert transformer. The Hilbert transformer derives the analytical signal of the input and is necessary for single sideband modulation. We computed a 10th order Hilbert transformer, which was designed with the equiripple algorithm and implement it in software (Appendix A) on the microcontroller.

Effect on Feedback Stability

If we assume an ideal frequency shifter, so that the ouput of the microcontroller is shifted by $s_0 = e^{j2\pi f_0}$, then the output ($Y_{acc}(s)$) of the closed loop system (figure 3.3) can be described with

$$Y_{acc} = L(s - s_0)U(s - s_0) + \big(L(s)Y_{acc}(s)\big) * \delta(s - s_0) \tag{3.7}$$

where $U(s)$ is the input, and $L(s)$ the open loop transfer function. This yields the system equation

$$Y_{acc} - \big(L(s)Y_{acc}(s)\big) * \delta(s - s_0) = L(s - s_0)U(s - s_0) \tag{3.8}$$

$$Y_{acc}\big[1 - L(s - s_0)\delta(s - s_0) * (\cdot)\big] = L(s - s_0)U(s - s_0) \tag{3.9}$$

After long division we find

$$Y_{acc} = L(s - s_0)U(s - s_0) + L(s - s_0)L(s - 2s_0)U(s - 2s_0) + \cdots \tag{3.10}$$

From the closed loop system description (eq. 3.10) we can deduce that after N trips through the feedback loop an input signal $U(s)$ becomes

$$U(s - Ns_0)\prod_{i=1}^{N} L(s - is_0) \tag{3.11}$$

We can see (eq. 3.11) that the rate at which signals decay in the closed loop system depends not only on the amplitude of the open-loop transfer function in the frequency range of the original signal, but on the rest of the transfer function as well. The multiplication of different regions of $L(s)$ has the effect that peaks and notches of $L(s)$ are smoothed in the closed-loop system response. The frequencies for which the gain of $L(s)$ is high are the frequencies where instability will likely occur first. Frequency shifting ensures that the gains at these frequencies are closer to the average gain of $L(s)$ in the closed-loop system response. This increases the forward path gain at which instability will occur and therefore increases usable gain.

In the absence of a model of the open loop response $L(s)$, little can be said about the ideal value for the frequency shift, f_0, but it is important to note that for frequency

shifting to be most effective the width of the peaks and notches must be smaller than f_0. However, a large frequency shift will also significantly alter the spectral characteristics of the signal, which is not desirable. We will test different values and empirically determine a good value.

3.5 Stability Assessment: Empirical Method

In empirical testing, it is straightforward to determine if the system has become unstable. We designed a simple test configuration to empirically evaluate the gain margin in our system, and particularly the additional usable gain that is achievable with the implemented feedback suppression methods. The wearable devices were mounted on the user with the actuator mounted on the intermediate phalanx (left 3.1). The user was then asked to execute the full range of motion of the index finger, that is, full extension to full flexion. This was done three times and the average energy received by the accelerometer was calculated. This trial was done for every method tested and a wide range of gains. The system was determined to be unstable if ratio of the energy received, E, by the square of the gain A exceeded an empirically determined threshold, P

$$\frac{E}{A^2} > P \tag{3.12}$$

Empirically, this occurred when the actuator shook violently due to unstable feedback.

3.6 Results

The results from the energy measurements tests are shown in figure 3.8. The stability measure E/A^2 increased rapidly after attaining a maximum stable gain value. At this

level, the feedback instability saturates the actuator capability for large portions of the trials. Prior to this, the measure E/A^2 remained relatively constant for all methods, suggesting little effect of feedback instability on the signal. While gain levels vary quite significantly in the 5 different setups tested, the instability patterns are similar. All methods show a steep slope at the point of instability, where E/A^2 increases with 15-30dB with only a 1 dB increase in A. The actual slopes are likely even steeper than the data indicates as A was increased with 1 dB every trial.

The calculated additional usable gains for each method are displayed in figure 3.9. The actuator compensation method gave 4 dB of additional usable gain. The frequency shifting method gave better results, 4 dB, 7 dB and 10 dB for 40Hz, 80Hz and 120Hz frequency shifts, respectively. Interestingly, the additional usable gain in dB achieved with the frequency shift methods seems to scale linearly with the size of the frequency shifts.

3.7 Discussion

As we can see in figure 3.9, all four tested methods provide at least 4 dB of additional usable gain which is a significant improvement over not using any feedback suppression method. Although the actuator compensation method provided an additional 4 dB of usable gain, the perceived effect of the touch amplification seems to suffer with this method. This can be because important frequencies for perceiving touch are in the frequency range that are attenuated by this method. The three different frequency shifting implementations show that a larger frequency shift results in a larger maximum usable gain. This is consistent with previous literature. Larger frequency shifts do noticeably affect the characteristics of the signal. For 120 Hz frequency shifting, users reported the feedback felt less natural than 80 Hz or 40 Hz frequency shifting.

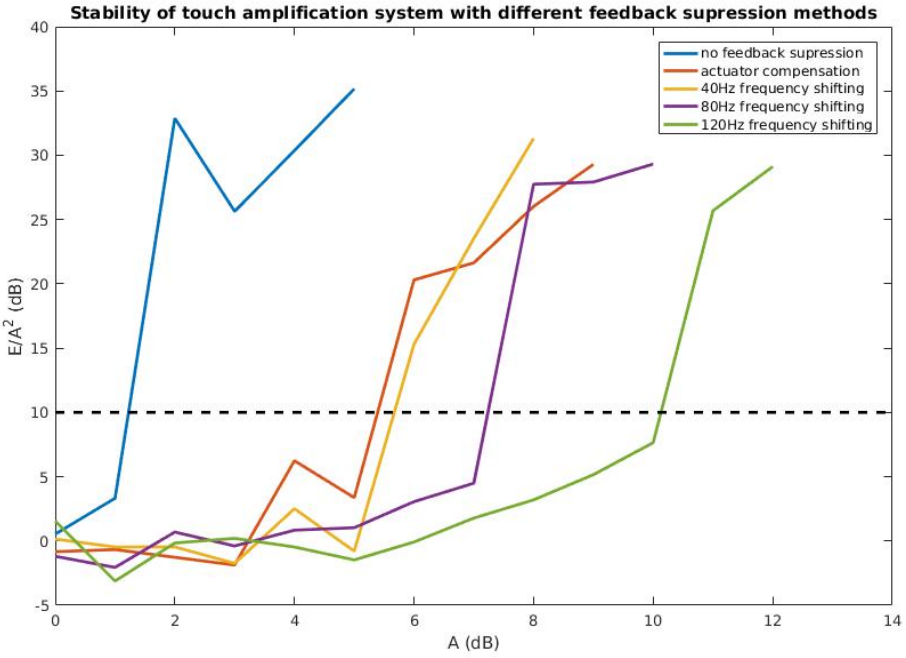

Figure 3.8: A specific motion was executed for each method and a range of forward path gains (A, or 20 $log_{10}(A)$ in dB). For each trial the energy of the vibrations on the fingertip (E, or $10\log_{10}(E)$ in dB) was recorded. If the ratio, $\frac{E}{A^2}$, was above a certain threshold the system was deemed unstable. This stability threshold is represented by the horizontal dashed line.

80 Hz frequency shifting was determined to be the best method tested. At this setting the perceived haptic feedback was very natural and the 7 dB of additional usable gain allowed the device to use gain settings that are high enough to generate sufficiently large haptic feedback for most applications with the actuator mounted on the intermediate phalanx.

3.8 Applications

For augmented reality applications the effect of the touch amplification device must be configured according to the position of the finger. The finger is tracked using a motion capture system and depending on the location, we send specific configurations to

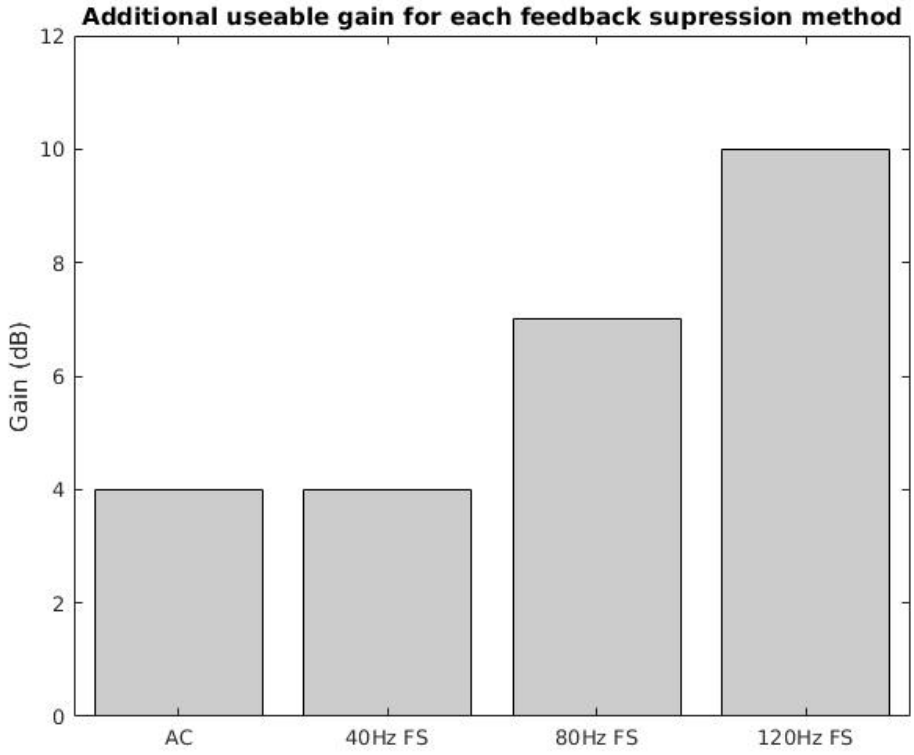

Figure 3.9: Comparison of additional gain that can be implemented without causing instability for the four methods tested: actuator compensation(AC), 40 Hz frequency shifting(40 Hz FS), 80 Hz frequency shifting (80 Hz FS) and 120 Hz frequency shifting (120 Hz FS).

the touch amplification system to change the way interacting with the world feels. The mirco-controller implements a parametrized biquad filter on the signal to the actuator. The parameters of this biquad filter are sent over Wi-Fi in real time to the microcontroller. This allows the virtual environment to change some basic signal parameters of the touch amplification system. Cutoff frequencies, filter type and gain can be controlled from the virtual environment on the PC. These parameters allow additional control over how touch is augmented and could make surfaces feel harder, softer, rougher, smoother, or even textured, similar to the methods used by Culbertson et al [9].

One of the proposed applications for this is a virtual keyboard depicted in figure

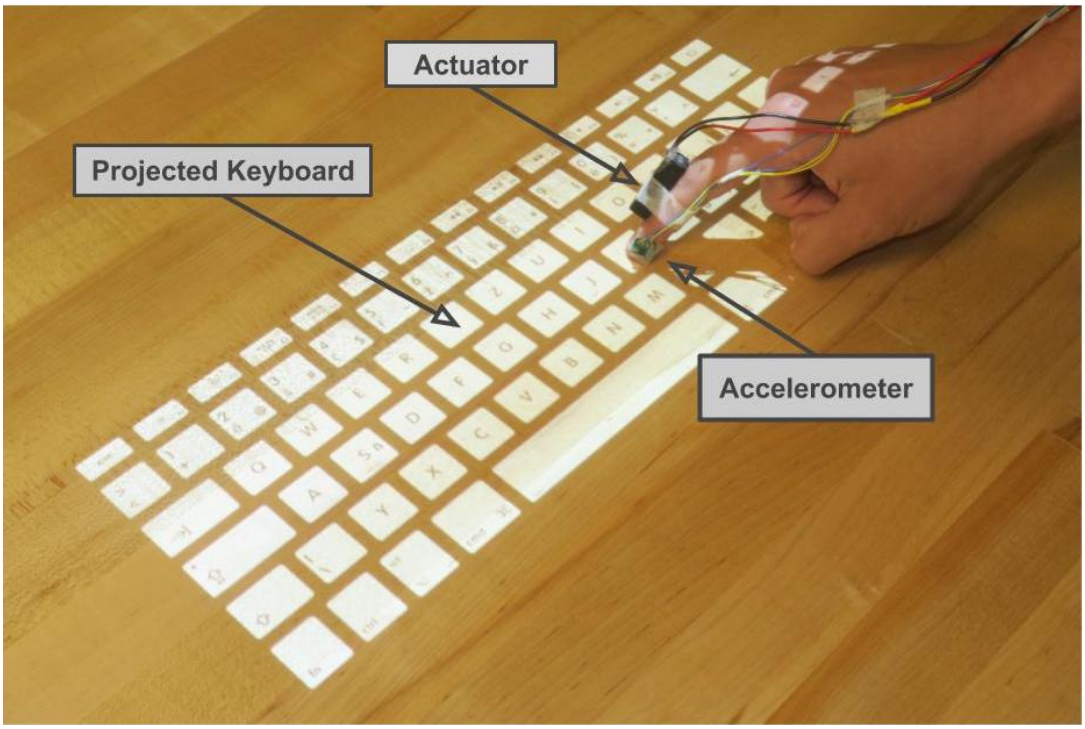

Figure 3.10: Virtual keyboard that can be recreated on any surface with the touch amplification device.

3.10. When the motion capture system detects that the fingertip is over a key, the touch amplification system will be active. This results in the user feeling amplified sensation when tapping on the keys as opposed to tapping on the non-augmented surface. This provides the user with an intuitive and enjoyable experience when pressing keys on the virtual keyboard. Additionally, the added feedback gives the user confidence that the key has been successfully pressed. This is similar to haptic feedback on touch screen keyboards on smartphones. However, this system does not need a touch screen surface to function and touch amplification provides more natural feedback as it preserves the characteristic structure of the touch interaction.

Another application that has already been successfully implemented involves a virtual calculator projected onto a flat surface with virtual keys, similar to the virtual keyboard described above. The user can tap the buttons of the calculator and use it as a normal

calculator.

Chapter 4

Conclusions

This thesis proposes a wearable electronic interface that provides haptic feedback to the hand, in the form of touch-dependent vibrations, when users are touching real surfaces, in order to simulate the perceptual experience of touching different objects or materials. In order to render touch feedback that is more realistic than can be achieved with synthesized (simulated) signals, an approach is proposed in which contact-dependent vibrations felt by the hand are amplified and modified in real time in order to affect what the hand feels.

One challenge addressed in this thesis is that the performance of the device is greatly affected by the continuum mechanics of the body tissues through which these touch dependent vibrations propagate, as mechanical waves. An analysis of the propagation of these waves in the finger revealed complex spatial and frequency dependencies that defied a simple modeling approach. It appeared to be prohibitively challenging to create a model for wave propagation in the finger that accounts for all the different contact conditions and finger postures that occur during manual touch. Nonetheless, the results provided insight into factors that are important for the design of an electronic display like the one envisioned here.

Chapter 3 presented a unique electronic system for touch amplification, including hardware, digital, and analog signal processing. Due to the presence of feedback instabilities in this system, this chapter also investigated methods for feedback suppression that could increase the feasible range of amplification gains of the system without recourse to channel estimation, which, based on the results of Chapter 2, appeared to be very difficult to achieve.

The touch amplification system designed in Chapter 3 can augment real surfaces with virtual objects. Although not emphasized in this thesis, a versatile software framework allows the touch amplification device to be quickly and easily configured for different applications. Chapter 3 also describes a virtual keyboard application. This virtual keyboard can be interacted with naturally and provides realistic haptic feedback when the keys are depressed.

4.1 Contributions

The experiments from Chapter 2 contribute some of the first results on the propagation of touch elicited elastic waves in the finger. The chapter also mapped the dependence of these processes on contact conditions and different finger postures. This provides essential knowledge for the understanding of touch perception and tactile waves, and basic guidelines for the design of haptic devices that use touch related vibrations. The results demonstrate complex patterns of vibration propagation, from the fingertip to remote locations on the finger. It was shown that vibrotactile waves traveling through the finger in the 100- 200 Hz range are often attenuated as little as 3 dB when traveling through the entire length of the finger. In contrast, vibrations in the frequency above 200 Hz are attenuated much more significantly when traveling throughout the finger and their propagation is consistently influenced by contact conditions of the fingers. This implies

that during a simple interaction, such as a tap on a hard surface, the wave propagation characteristics vary significantly.

Chapter 3 presented a preliminary design of a touch amplification device, motivated by an augmented reality example. Chapter 3 also analysed feedback suppression methods suited to such a device. I show that simple feedback suppression methods, conventionally used for audio systems, can significantly improve the performance of a touch amplification device. The analyses of these feedback suppression algorithms for haptic devices identify the usable gain enabled and the tradeoffs involved. Frequency shifting can provide up to 10 dB of additional usable gain, which is sufficient for many of the proposed applications for touch amplification. A flexible software framework that was built enables the system to be used for a variety of different applications. Parameters that can easily be configured over Wi-Fi allow in-depth control of the effects of touch amplification. This allows the sensation of a touch interaction with an object to be altered dynamically.

4.2 Discussion and Future Implications

The results and conclusions from Chapter 2 provide some insight into patterns of wave propagation in the finger and how contact conditions affect the wave propagation – information that could be profitably used in future haptic display devices. However, several questions remain. It is not entirely clear how different hand postures affect wave propagation. More measurements with a larger variety of finger postures and contact conditions could shed more light on this. While it is challenging to create an accurate model for the wave propagation in the finger at the moment, additional research might make this possible. Such a model would be a useful tool for designing haptic devices.

This thesis focused on simple feedback suppression methods. More refined techniques often involve estimating the physical feedback path through the finger dynamically, with

the use of adaptive filters. One challenge in adopting such approaches is that the transmission path in the finger is variable and no simple analytical model exists for this. However, additional work could rectify these issues, perhaps enabling devices that use higher gain levels.

Currently, the tested applications consist of simple augmented reality demonstrations. The results from this thesis suggest unique applications for touch amplification in this area. In addition, although not emphasized in this thesis, touch amplification could improve the capabilities of human touch. If experiments with this application are successful, wearable haptic devices such as this could provide humans with superhuman dexterity or the ability to feel otherwise undetectable haptic cues. Additionally, touch amplification devices could artificially restore the sense of touch in people suffering from a peripheral sensory impairment due to disease, such as Type II diabetes, in much the same way that a hearing aid is able to address auditory deficits.

Appendix A

Microcontroller Code

```
#include <Wire.h>
#include <ESP8266WiFi.h>
#include <WiFiUdp.h>

#define LIS3DSH_ADDR 0x1E //accelerometer address
#define MCP4725_ADDR 0x62 //DAC address


// wifi connection variables
const char* ssid = "Retouch_Experimental";
const char* password = "********";
boolean wifiConnected = false;



// UDP variables
unsigned int localPort = 123;
WiFiUDP UDP;
boolean udpConnected = false;
char packetBuffer[UDP_TX_PACKET_MAX_SIZE];
char ReplyBuffer[] = "acknowledged";



int mult_with_sin_freq = 80;
int freq_signal_gen = 130;
int ssbm_freq = 80;
int operation_mode = 1;
double amplification = 1.0;
int minLoopTime = 625;
int noise_treshold = 0;//700;
short x,y,z;
int t;
int i;
```

```
int impulse_counter = 0;
int sin_counter_mult=0;
int sin_counter_shift=0;
int cos_counter_shift=0;
int noise_counter=0;
int x_int,x_int_raw, y_int,z_int;
int raw_signal;
int post_filter_signal;
unsigned long startTime;
unsigned long loopTime;
double input_freq_shift[11]= {0,0,0,0,0,0,0,0,0,0,0};
double input_comb_filt[11]= {0,0,0,0,0,0,0,0,0,0,0};
double output_comb_filt[11]= {0,0,0,0,0,0,0,0,0,0,0};
double output_high_pass_filter_input[3]= {0,0,0};
double hilbert_coeffs[11] = {-0.092,-0.0234, ...};
double output_band_pass_filter[3]= {0,0,0};
double input_biquad_filter[2] = {0,0};
double output_biquad_filter[2] = {0,0};
double input_high_pass_filter_input[3]= {0,0,0};
double input_band_pass_filter[3]= {0,0,0};
double input_low_pass_filter_output[3] = {0,0,0};
double output_low_pass_filter_output[3] = {0,0,0};
double output_high_pass_filter_output[3] = {0,0,0};
double input_high_pass_filter_output[3] = {0,0,0};
double bandpassed_inputs[50];
const double pi = 3.14;
int low_pass_cutoff = 10;
int high_pass_cutoff = 120 ;
int output_mult_with_sin = 0;
int output_mult_with_noise = 0;
float biquad_a0;
float biquad_a1;
float biquad_a2;
float biquad_b1;
float biquad_b2;
boolean biquad_on = false;
int output_biquad;
int bandpassed_inputs_counter = 0;
int sin_counter_signal_gen;
double bandpassed_acc = 0;
boolean actuator_off = true;
double bandpassed_signal = 0;
double hilbert_transformed;
int output_freq_shift = 0;
int sin_counter_test_signal = 0;


//filter
//This is a 2nd order High pass with a 30hz cutoff
// SOS =
// [1 -2  1 1 -1.8337 0.8465]
```

```
//
// G =
// [0.9201  1]
//
//This is a 2nd order High pass with a 10hz cutoff
// SOS =
// [1  -2  1 1 -1.9556 0.9565]
//
// G =
// [0.9780  1]

double b01_1 = 1;
double b11_1 = -2;
double b21_1 = 1;
double a11_1 = -1.8337;
double a21_1 = 0.8465;
double g1_1 = 0.9201;
double g2_1 = 1;




//filter
//This is a 2nd order band pass with a 35-55 cutoff
// SOS =
// [1  0 -1  1 -1.89588278428643 0.924390491658207]
// G =
// [0.037804754170896  1]

double b01_2 = 1;
double b11_2 = 0;
double b21_2 = 1;
double a11_2 = -1.89588278428643;
double a21_2 = 0.924390491658207;
double g1_2 = 0.037804754170896;
double g2_2 = 1;




//filter
//This is a 2nd order low pass with a 250 cutoff
// SOS =
// [1 2 1 1 -0.699738028273366  0.259495175740772]
// G =
// [0.139939286866852  1]

double b01_3 = 1;
double b11_3 = 2;
double b21_3 = 1;
double a11_3 = -0.699738028273366;
```

```
double a21_3 = 0.259495175740772;
double g1_3 = 0.139939286866852;
double g2_3 = 1;



//filter
//This is a 2nd order high pass with a 160 cutoff
// SOS =
// [1 -2 1 1 -1.142980502539901  0.412801598096189]
// G =
// [0.638945525159023 1]

double b01_4 = 1;
double b11_4 = -2;
double b21_4 = 1;
double a11_4 = -1.142980502539901;
double a21_4 = 0.412801598096189;
double g1_4 = 0.638945525159023;
double g2_4 = 1;


//The sin fucntions seem to have issues so we use lookup tables
const double sin_lookup_80hz[20] =
{0,0.309,0.587,0.809,...};


const double sin_lookup_10hz[160] =
{0,0.039,0.078,0.118,0.157, ...}



void setup()
{

Wire.begin();           // join i2c bus (address optional for master)
Wire.setClock(400000); // Set I2c speed  to fast
Serial.begin(230400);  // start serial for output
Wire.beginTransmission(LIS3DSH_ADDR); // transmit to accelerometer
//Send address of 'Control register 4' to write configurations
Wire.write(0x20);
Wire.write(0x9F);//Write a value that enables x,y,z accelerometers
Wire.endTransmission();// stop transmitting

Wire.beginTransmission(LIS3DSH_ADDR); // transmit to device #30
Wire.write(0x24);//Send address of register 5 to write configuration
Wire.write(0x18);//Write the scale to +/-8g
Wire.endTransmission();// stop transmitting
```

```
// Initialise wifi connection
wifiConnected = connectWifi();

// only proceed if wifi connection successful
if(wifiConnected){
udpConnected = connectUDP();
if (udpConnected){
// initialise pins
pinMode(LED_BUILTIN,OUTPUT);
}
}




}

void loop()
{



startTime = micros(); // Measure time when loop starts



//Read acc values
Wire.beginTransmission(LIS3DSH_ADDR); // transmit to device
//Send address of LSB of x. Address is auto-increased after each reading.
Wire.write(0x28);
Wire.endTransmission();     // stop transmitting
// request 6 bytes from slave device #30
Wire.requestFrom(LIS3DSH_ADDR, 6);
x = Wire.read() | Wire.read()<<8; //x acceleration
y = Wire.read() | Wire.read()<<8; //y acceleration
z = Wire.read() | Wire.read()<<8; //z acceleration



//Output modes

// Output Off
if (operation_mode == 0) {
post_filter_signal = 0;
//Regular amplification
} else if (operation_mode == 1){
raw_signal =x;
post_filter_signal =amplification*high_pass_filter_input(raw_signal);
post_filter_signal = freq_shift(post_filter_signal,ssbm_freq);
post_filter_signal = low_pass_filter_output(post_filter_signal);
```

```
//Mask with sine wave
} else if (operation_mode == 2){
if (sin_counter_signal_gen >= 160){
sin_counter_signal_gen -= 160;
}
post_filter_signal = (int) 5000*sin_lookup_10hz[sin_counter_signal_gen];
sin_counter_signal_gen += (freq_signal_gen/10);
//Raw x
} else if (operation_mode == 3){
raw_signal =x;
post_filter_signal =amplification*high_pass_filter_input(raw_signal);
//SSBM with x
} else if (operation_mode == 4){
raw_signal =x;
post_filter_signal =amplification*high_pass_filter_input(raw_signal);
post_filter_signal = freq_shift(post_filter_signal,ssbm_freq);
//SSBM x with BW limit
} else if (operation_mode == 5){
raw_signal =x;
post_filter_signal =amplification*high_pass_filter_input(raw_signal);
post_filter_signal = freq_shift(post_filter_signal,ssbm_freq);
post_filter_signal = low_pass_filter_output(post_filter_signal);
//high pass x
} else if (operation_mode == 6){
raw_signal =x;
post_filter_signal =amplification*high_pass_filter_input(raw_signal);
post_filter_signal = high_pass_filter_output(post_filter_signal);
}



if (biquad_on){
post_filter_signal = biquad_filter(post_filter_signal);
}


//filter out noise
if((abs(post_filter_signal) < noise_treshold)){
post_filter_signal = 0;
}


if (post_filter_signal > 4094){
post_filter_signal = 4094;
}
if (post_filter_signal < 1){
post_filter_signal = 1;
}
//Write filtered values
Wire.beginTransmission(MCP4725_ADDR);
Wire.write(64);    // cmd to update the DAC
```

```
Wire.write(post_filter_signal >> 4);  // the 8 most significant bits
Wire.write((post_filter_signal & 15) << 4); // the 4 least significant bits
Wire.endTransmission();




// check if the WiFi and UDP connections were successful
if(wifiConnected){
if(udpConnected){
// if there s data available, read a packet
int packetSize = UDP.parsePacket();
if(packetSize) {
Serial.println("packet_received");
Serial.println(packetBuffer);
IPAddress remote = UDP.remoteIP();
// read the packet into packetBufffer
memset(&packetBuffer[0],0,UDP_TX_PACKET_MAX_SIZE);
UDP.read(packetBuffer,UDP_TX_PACKET_MAX_SIZE);
loopTime = micros() - startTime;
String packetBuffer_string = (String) packetBuffer;
if (packetBuffer[0] == 'J'){
int firstComma = packetBuffer_string.indexOf(',');
operation_mode = (packetBuffer_string.substring(firstComma+1)).toInt();
}else if (packetBuffer[0] == 'S'){
firstComma =
packetBuffer_string.indexOf(',');
secondComma =
packetBuffer_string.substring(firstComma+1).indexOf(',') + firstComma+1;
thirdComma =
packetBuffer_string.substring(secondComma+1).indexOf(',') + secondComma+1;
fourthComma =
packetBuffer_string.substring(thirdComma+1).indexOf(',') + thirdComma+1;
operation_mode =
packetBuffer_string.substring(firstComma+1, secondComma+1).toInt();
amplification =
packetBuffer_string.substring(secondComma+1, thirdComma+1).toFloat();
ssbm_freq =
packetBuffer_string.substring(thirdComma+1).toInt();
}else if (packetBuffer[0] =='X'){
amplification  = (packetBuffer_string.substring(1, 2)).toInt();
if(packetBuffer[3] != 'H'){
firstComma = packetBuffer_string.indexOf(',');
secondComma =
packetBuffer_string.substring(firstComma+1).indexOf(',') + firstComma+1;
thirdComma =
packetBuffer_string.substring(secondComma+1).indexOf(',') + secondComma+1;
fourthComma =
packetBuffer_string.substring(thirdComma+1).indexOf(',') + thirdComma+1;
```

```
fifthComma =
packetBuffer_string.substring(fourthComma+1).indexOf(',') + fourthComma+1;
sixthComma =
(acketBuffer_string.substring(fifthComma+1).indexOf(',') + fifthComma+1;
seventhComma =
packetBuffer_string.substring(sixthComma+1).indexOf(',') + sixthComma+1;
biquad_a0 =
(packetBuffer_string.substring(firstComma+1, secondComma+1)).toFloat();
biquad_a1 =
(packetBuffer_string.substring(secondComma+1, thirdComma+1)).toFloat();
biquad_a2 =
(packetBuffer_string.substring(thirdComma+1, fourthComma+1)).toFloat();
biquad_b1 =
(packetBuffer_string.substring(fourthComma+1, fifthComma+1)).toFloat();
biquad_b2 =
(packetBuffer_string.substring(fifthComma+1, sixthComma+1)).toFloat();
mult_with_sin_freq =
(packetBuffer_string.substring(sixthComma+1,seventhComma+1)).toInt();
operation_mode =
(packetBuffer_string.substring(seventhComma+1)).toInt();
biquad_on = true;
}
else {
biquad_on = false;
}
}
}
}
}









while (micros() - startTime < minLoopTime){
}
loopTime = micros() - startTime;
//Serial.println(loopTime);
if (loopTime > minLoopTime+10) {
digitalWrite(LED_BUILTIN, HIGH);
} else {
digitalWrite(LED_BUILTIN, LOW);
}



}
```

```
// Mulitply with a sine wave of specific frequency,  because of
// lookup table issues frequencies below 10Hz will not work,
// and all are approximate
int mult_with_sin(int newest_input,int freq){
if (sin_counter_mult >= 160){
sin_counter_mult -= 160;
}
output_mult_with_sin = (int) newest_input*sin_lookup_10hz[sin_counter_mult];
sin_counter_mult += (freq/10);
return output_mult_with_sin;
}


int high_pass_filter_input(int newest_input){
input_high_pass_filter_input[0] = input_high_pass_filter_input[1];
input_high_pass_filter_input[1] = input_high_pass_filter_input[2];
input_high_pass_filter_input[2] = g1_1*newest_input;

output_high_pass_filter_input[0] = output_high_pass_filter_input[1];
output_high_pass_filter_input[1] = output_high_pass_filter_input[2];
output_high_pass_filter_input[2] =
g2_1*(b01_1*input_high_pass_filter_input[2] +
b11_1*input_high_pass_filter_input[1] +
b21_1*input_high_pass_filter_input[0]) -
a11_1*output_high_pass_filter_input[1] -
a21_1*output_high_pass_filter_input[0];

return (int) g2_1*output_high_pass_filter_input[2];
}


int low_pass_filter_output(int newest_input){
input_low_pass_filter_output[0] = input_low_pass_filter_output[1];
input_low_pass_filter_output[1] = input_low_pass_filter_output[2];
```

```
input_low_pass_filter_output[2] = g1_3*newest_input;

output_low_pass_filter_output[0] = output_low_pass_filter_output[1];
output_low_pass_filter_output[1] = output_low_pass_filter_output[2];
output_low_pass_filter_output[2] =
 g2_3*(b01_3*input_low_pass_filter_output[2] +
 b11_3*input_low_pass_filter_output[1] +
 b21_3*input_low_pass_filter_output[0]) -
 a11_3*output_low_pass_filter_output[1] -
 a21_3*output_low_pass_filter_output[0];

return (int) g2_3*output_low_pass_filter_output[2];
}

int high_pass_filter_output(int newest_input){
input_high_pass_filter_output[0] = input_high_pass_filter_output[1];
input_high_pass_filter_output[1] = input_high_pass_filter_output[2];
input_high_pass_filter_output[2] = g1_4*newest_input;

output_high_pass_filter_output[0] = output_high_pass_filter_output[1];
output_high_pass_filter_output[1] = output_high_pass_filter_output[2];
output_high_pass_filter_output[2] =
g2_4*(b01_4*input_high_pass_filter_output[2] +
b11_4*input_high_pass_filter_output[1] +
b21_4*input_high_pass_filter_output[0]) -
a11_4*output_high_pass_filter_output[1] -
a21_4*output_high_pass_filter_output[0];

return (int) g2_4*output_high_pass_filter_output[2];
}


int biquad_filter(int newest_input){

output_biquad = biquad_a0*newest_input +
biquad_a1*input_biquad_filter[0] +
biquad_a2*input_biquad_filter[1] -
biquad_b1*output_biquad_filter[0] -
biquad_b2*output_biquad_filter[1];

//update all values
input_biquad_filter[1] = input_biquad_filter[0];
input_biquad_filter[0] = newest_input;
output_biquad_filter[1] = output_biquad_filter[0];
output_biquad_filter[0] = output_biquad;

return (int)output_biquad;
}
```

```
int freq_shift(int newest_input,int freq){

//Input the new input into the array of inputs
i = 0;
while (i < 10){
input_freq_shift[i] = input_freq_shift[i+1];
i = i+1;
}
input_freq_shift[10] = (double) newest_input;

hilbert_transformed = 0;
i=0;
while (i < 11){
hilbert_transformed =
hilbert_transformed +
input_freq_shift[10-i]*hilbert_coeffs[i];
i=i+1;
}
if (sin_counter_shift >= 160){
sin_counter_shift -= 160;
}
if (cos_counter_shift >= 160){
cos_counter_shift -= 160;
}
if (cos_counter_shift < 0){
cos_counter_shift += 160;
}
output_freq_shift =
input_freq_shift[5]*sin_lookup_10hz[cos_counter_shift] -
hilbert_transformed*sin_lookup_10hz[sin_counter_shift];
sin_counter_shift += (freq/10);
cos_counter_shift =  40-sin_counter_shift;
return (int) output_freq_shift;
}



// connect to UDP     returns true if successful or false if not
boolean connectUDP(){
boolean state = false;

Serial.println("");
Serial.println("Connecting to UDP");

if(UDP.begin(localPort) == 1){
Serial.println("Connection successful");
state = true;
}
else{
Serial.println("Connection failed");
}
```

```
return state;
}


// connect to wifi     returns true if successful or false if not
boolean connectWifi(){
boolean state = true;
int i = 0;
WiFi.begin(ssid, password);
Serial.println("");
Serial.println("Connecting to WiFi");

// Wait for connection
Serial.print("Connecting");
while (WiFi.status() != WL_CONNECTED) {
delay(500);
Serial.print(".");
if (i > 100){
state = false;
break;
}
i++;
}
if (state){
Serial.println("");
Serial.print("Connected to ");
Serial.println(ssid);
Serial.print("IP address: ");
Serial.println(WiFi.localIP());
}
else {
Serial.println("");
Serial.println("Connection failed.");
}
return state;
}
```

Bibliography

[1] S. Adewusi, S. Rakheja, P. Marcotte, and J. Boutin. Vibration transmissibility characteristics of the human hand–arm system under different postures, hand forces and excitation levels. *Journal of sound and vibration*, 329(14):2953–2971, 2010.

[2] O. Bau, I. Poupyrev, A. Israr, and C. Harrison. Teslatouch: electrovibration for touch surfaces. In *Proceedings of the 23nd annual ACM symposium on User interface software and technology*, pages 283–292. ACM, 2010.

[3] E. Berdahl and D. Harris. Frequency shifting for acoustic howling suppression. In *Proceedings of the 13th International Conference on Digital Audio Effects, Graz, Austria*, volume 610, 2010.

[4] M. Biet, F. Giraud, and B. Lemaire-Semail. Implementation of tactile feedback by modifying the perceived friction. *The European Physical Journal Applied Physics*, 43(1):123–135, 2008.

[5] D. K. Bustamante, T. L. Worrall, and M. J. Williamson. Measurement and adaptive suppression of acoustic feedback in hearing aids. In *Acoustics, Speech, and Signal Processing, 1989. ICASSP-89., 1989 International Conference on*, pages 2017–2020. IEEE, 1989.

[6] W. Buxton, R. Hill, and P. Rowley. Issues and techniques in touch-sensitive tablet input. *ACM SIGGRAPH Computer Graphics*, 19(3):215–224, 1985.

[7] J. Chalupper, T. A. Powers, and A. Steinbuss. Combining phase cancellation, frequency shifting, and acoustic fingerprint for improved feedback suppression. *Hearing review*, 18(1):24–29, 2011.

[8] M. Chartier, N. Thomas, Y. Shao, and Y. Visell. Toward a wearable tactile sensory amplification device: Transfer characteristics and optimization.

[9] H. Culbertson and K. J. Kuchenbecker. Importance of matching physical friction, hardness, and texture in creating realistic haptic virtual surfaces. *IEEE Transactions on Haptics*, 10(1):63–74, 2017.

[10] H. Culbertson, J. M. Romano, P. Castillo, M. Mintz, and K. J. Kuchenbecker. Refined methods for creating realistic haptic virtual textures from tool-mediated contact acceleration data. In *Haptics Symposium (HAPTICS), 2012 IEEE*, pages 385–391. IEEE, 2012.

[11] B. Delhaye, V. Hayward, P. Lefèvre, and J.-L. Thonnard. Texture-induced vibrations in the forearm during tactile exploration. 2012.

[12] C. Forlines and R. Balakrishnan. Evaluating tactile feedback and direct vs. indirect stylus input in pointing and crossing selection tasks. In *Proceedings of the SIGCHI Conference on Human Factors in Computing Systems*, pages 1563–1572. ACM, 2008.

[13] M. Fukumoto and T. Sugimura. Active click: tactile feedback for touch panels. In *CHI'01 Extended Abstracts on Human Factors in Computing Systems*, pages 121–122. ACM, 2001.

[14] J. E. Greenberg, P. M. Zurek, and M. Brantley. Evaluation of feedback-reduction algorithms for hearing aids. *The Journal of the Acoustical Society of America*, 108(5):2366–2376, 2000.

[15] R. S. Johansson and J. R. Flanagan. Coding and use of tactile signals from the fingertips in object manipulation tasks. *Nature Reviews Neuroscience*, 10(5):345–359, 2009.

[16] L. A. Jones and S. J. Lederman. *Human hand function*. Oxford University Press, 2006.

[17] J. C. Lee, P. H. Dietz, D. Leigh, W. S. Yerazunis, and S. E. Hudson. Haptic pen: a tactile feedback stylus for touch screens. In *Proceedings of the 17th annual ACM symposium on User interface software and technology*, pages 291–294. ACM, 2004.

[18] X. Libouton, O. Barbier, Y. Berger, L. Plaghki, and J.-L. Thonnard. Tactile roughness discrimination of the finger pad relies primarily on vibration sensitive afferents not necessarily located in the hand. *Behavioural brain research*, 229(1):273–279, 2012.

[19] T. Maeda, R. Peiris, N. Masashi, Y. Tanaka, and K. Minamizawa. Hapticaid: wearable haptic augmentation system for enhanced, enchanted and empathised haptic experiences. In *SIGGRAPH ASIA 2016 Emerging Technologies*, page 4. ACM, 2016.

[20] T. Maeda, K. Tsuchiya, R. Peiris, Y. Tanaka, and K. Minamizawa. Hapticaid: Haptic experiences system using mobile platform. In *Proceedings of the Tenth International Conference on Tangible, Embedded, and Embodied Interaction*, pages 397–402. ACM, 2017.

[21] L. R. Manfredi, A. T. Baker, D. O. Elias, J. F. Dammann III, M. C. Zielinski, V. S. Polashock, and S. J. Bensmaia. The effect of surface wave propagation on neural responses to vibration in primate glabrous skin. *PLoS One*, 7(2):e31203, 2012.

[22] J. L. Nielsen and U. P. Svensson. Performance of some linear time-varying systems in control of acoustic feedback. *The Journal of the Acoustical Society of America*, 106(1):240–254, 1999.

[23] H. Nyquist. Regeneration theory. *Bell Labs Technical Journal*, 11(1):126–147, 1932.

[24] M. A. Poletti. The stability of multichannel sound systems with frequency shifting. *The Journal of the Acoustical Society of America*, 116(2):853–871, 2004.

[25] I. Poupyrev and S. Maruyama. Tactile interfaces for small touch screens. In *Proceedings of the 16th annual ACM symposium on User interface software and technology*, pages 217–220. ACM, 2003.

[26] H. Schäfer, Z. Wells, Y. Shao, and Y. Visell. Transfer properties of touch elicited waves: Effect of posture and contact conditions. In *World Haptics Conference (WHC), 2015 IEEE*, pages xix–xix. IEEE, 2017.

[27] M. Schroeder. Improvement of acoustic-feedback stability by frequency shifting. *The Journal of the Acoustical Society of America*, 36(9):1718–1724, 1964.

[28] Y. Shao, V. Hayward, and Y. Visell. Spatial patterns of cutaneous vibration during whole-hand haptic interactions. *Proceedings of the National Academy of Sciences*, 113(15):4188–4193, 2016.

[29] K. O. Sofia and L. Jones. Mechanical and psychophysical studies of surface wave propagation during vibrotactile stimulation. *IEEE transactions on haptics*, 6(3):320–329, 2013.

[30] D. Troxel. Understanding acoustic feedback & suppressors. *Rane Corporation*, 2005.

[31] Y. Visell, K. A. Duraikkannan, and V. Hayward. A device and method for multimodal haptic rendering of volumetric stiffness. In *International Conference on Human Haptic Sensing and Touch Enabled Computer Applications*, pages 478–486. Springer, 2014.

[32] H.-Y. Yao, V. Hayward, and R. Ellis. A tactile magnification instrument for minimally invasive surgery. *Medical Image Computing and Computer-Assisted Intervention–MICCAI 2004*, pages 89–96, 2004.

[33] C. Zheng, C. Hofmann, X. Li, and W. Kellermann. Analysis of additional stable gain by frequency shifting for acoustic feedback suppression using statistical room acoustics. *IEEE Signal Processing Letters*, 23(1):159–163, 2016.